

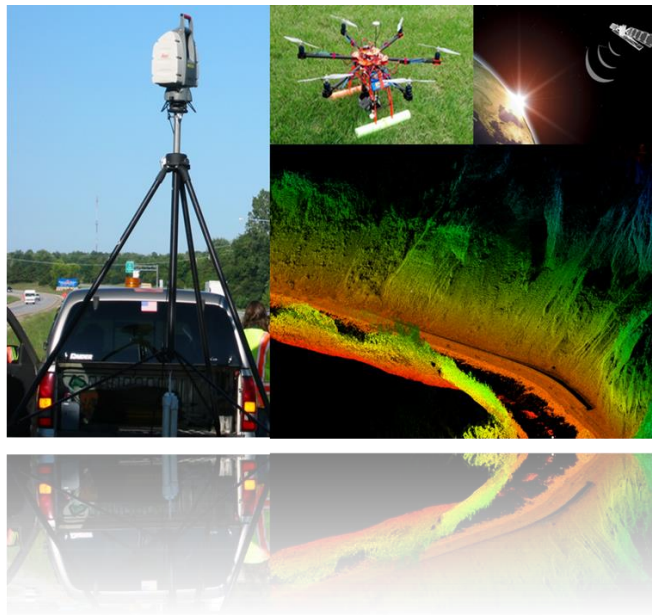
Deliverable 2-A: Candidate Remote Sensing Techniques for the Different Transportation Environments, Requirements, Platforms, and Optimal Data Fusion Methods for Assessing the State of Geotechnical Assets

Rudiger Escobar Wolf, El Hachemi Bouali, Thomas Oommen, Daniel Cerminaro, Keith W. Cunningham, Rick Dobson, and Colin Brooks

Michigan Technological University

USDOT Cooperative Agreement No. RITARS-14-H-MTU

Due on: December 15, 2014



Principal Investigator: **Dr. Thomas Oommen, Assistant Professor**

Department of Geological and Mining Engineering and Sciences

Michigan Technological University

1400 Townsend Drive

Houghton, MI 49931

(906) 487-2045

toommen@mtu.edu

Program Manager: **Caesar Singh, P.E.**

Director, University Grants Program/Program Manager

OST-Office of the Assistant Secretary for Research and Technology

U.S. Dept. of Transportation

1200 New Jersey Avenue, SE, E35-336

Washington, DC 20590

(202) 366-3252

Caesar.Singh@dot.gov

Michigan Tech

TABLE OF CONTENTS

1. Executive summary.....	3
2. Introduction.....	4
3. Remote Sensing Techniques and Possible Platforms	6
3.1 Synthetic Aperture Radar	6
3.2 LiDAR.....	20
3.3 Optical Photogrammetry	25
4. Requirements of remote sensing techniques for geotechnical asset management for regional scale condition assessment	27
4.1 Synthetic Aperture Radar	27
4.2 LiDAR.....	29
4.3 Optical photogrammetry.....	30
5. Requirements of remote sensing techniques for geotechnical asset management for local scale performance monitoring.....	31
5.1 Synthetic Aperture Radar	31
5.2 LiDAR	32
5.3 Optical photogrammetry	34
6. Remote sensing technologies rating	37
7. Conclusion.....	43
8. References.....	44

GLOSSARY OF TERMS

AASHTO	American Association of State Highway and Transportation Officials
CCD	Charge-Coupled Devices
DEM	Digital Elevation Model
DSI	Distributed Scatterer Interferometry
ENVISAT	Environmental Satellite
ESA	European Space Agency
ERS-1	European Remote Sensing Satellite 1
ERS-2	European Remote Sensing Satellite 2
GHz	Giga-Hertz
GNSS	Global Navigation Satellite System
INS	Inertial Navigation System
InSAR	Interferometric Synthetic Aperture Radar
IR	Infrared
LiDAR	Light Detection and Ranging
LOS	Line of sight
MERIS	Medium Resolution Imaging Spectrometer
PSI	Persistent Scatterer Interferometry
PTA	Phase Triangulation Algorithm
RADARSAT-1	Radar Satellite 1
RAR	Real Aperture Radar
SAR	Synthetic Aperture Radar
SHP	Statistically Homogeneous Pixels
SLC	Single Complex Look
UAV	Unmanned aerial vehicle
USDOT/OST-R	US Department of Transportation, through the Office of the Assistant Secretary for Research and Technology

1. EXECUTIVE SUMMARY: DELIVERABLE 2-A

Geotechnical assets are a critical part of the transportation infrastructure. The current methods to quantitatively evaluate the condition and manage these assets are not adequate to meet the demands of the public and therefore, need improvement (AASHTO 2013). The primary reason for the inadequacy of current method is, it is qualitative and laborious.

In this study, we rate the three commercial remote sensing techniques (InSAR-Interferometric Synthetic Aperture Radar; LiDAR-Light Detection and Ranging; and Photogrammetry) likely to be able to meet the needs of users in different transportation environments for geotechnical asset management. The applicability of these techniques are evaluated for both regional based condition assessment as well as for local scale condition assessment. The regional scale condition assessment represents evaluating the condition of a large network of geotechnical assets along a corridor, whereas, the local scale condition assessment represents evaluating the condition of one geotechnical asset at a time. In the case of regional scale condition assessment, the InSAR technique shows great promise while the photogrammetry is economical and practical to operate for local scale conditional assessment.

Using a rating methodology developed specifically for assessing the applicability of these remote sensing techniques for geotechnical asset management, each techniques was rated for information content, data spatial density and ground resolution, data availability and time interval recurrence, accuracy, direct cost for data collection and analysis, indirect cost for data collection and analysis, and availability of historical data. Key findings from the evaluation indicate that there is no technique that has high rating for all criteria. In general, the photogrammetry method is the most cost effective and easy to process method, whereas, the InSAR method has the relatively low cost per km² and can provide mm scale accuracy. The LiDAR and photogrammetry are comparable except that the initial cost for LiDAR instrumentation can be significantly higher. The detailed rating results highlight the criteria of the remote sensing techniques that have potential to impact the current practices for geotechnical asset management, and also the ones that need additional sensor development and commercialization. Ongoing and future activities of this study will investigate the field performance of these remote sensing techniques for geotechnical asset management.

Acknowledgements

This work is supported by the US Department of Transportation, through the Office of the Assistant Secretary for Research and Technology (USDOT/OST-R). The views, opinions, findings, and conclusions reflected in this paper are the responsibility of the authors only and do not represent the official policy or position of the USDOT-OST-R, or any state or other entity. Additional information regarding this project can be found at www.mtri.org/geoasset

2. Introduction

Transportation asset management (Cambridge Systematics Inc, 2002) is becoming the standard paradigm for developing and operating transportation infrastructure in the United States (AASHTO, 2011). Although transportation asset management in its broadest sense covers all those aspects that could be related to transportation corridors, some of the less visible assets have taken longer to be recognized as crucial to the process and included in the management (Sanford, 2003; Stanley, 2011; Anderson, 2013), in part due to the difficulty in categorizing and inventorying such an extensive body of assets.

Vessely (2013) outlines the general characteristics of the transportation asset management as applied to geotechnical assets, i.e. geotechnical asset management. Key elements of a geotechnical asset management system include data collection and monitoring of the assets performance over time, developed on a multi-tier hierarchical structure. A wide range of geotechnical features can be included in the list of assets, including embankments, cut slopes, and retaining walls. A key characteristic to analyze about these geotechnical assets is their long term stability, as part of their overall performance.

Anderson et al. (2008) presents the case of geotechnical asset management of retaining walls, and discusses in detail the case of the National Park Service retaining wall inventory. The monitoring and performance assessment of the retaining walls in that case is based predominantly on visual inspections by engineers or technicians, who visit the retaining walls and collect a series of rather subjective data on the wall conditions and characteristics, e.g. performance, age, ductility, etc. Each of those characteristics are rated or graded by the inspector based on his or her experience and understanding of the different categories in the evaluation matrix. After rating and multiplying the values by relative weights that take into account the relative importance of the different categories, a final score is obtained, and this value can be compared with standard values, to give an idea of the general performance and state of the asset (the retaining wall in this case).

Although relatively easy to implement in practice (e. g. quick data collection and interpretation), such an approach requires periodic field visits and detailed visual data collection, but perhaps more concerning is the obvious subjectivity and potential lack of uniformity in the criteria used to do the rating, leading to a potentially inconsistent database of performance monitoring information, both over time for a given asset (as different analysts may have different criteria to rate the assets), and over space for all the assets in a given area.

Stanley et al. (2013) describe a similar but broader approach to geotechnical asset management of slopes in general, based on the idea of condition indices and performance measures. These indices and measures can be assigned based on visual inspection data, as for the case of retaining walls described by Anderson et al. (2008), but could also benefit from more quantitative information, linked to the geotechnical behavior of the asset. Managing the spatial characteristics of the geotechnical assets over the length of a transportation corridor segment, will also require integrating this information into a GIS database.

More in-depth and detailed data collection and analysis will obviously imply a much higher cost, and will not be justified unless the long term benefit outweighs the cost of conducting such data collection and analysis on a regular basis. Quantitative data that describe the physical, and more specifically geotechnical and mechanical state of the asset would be much more informative, but such methods are often too expensive to be applied over broad areas, in the absence of strong evidence for failure or high impact damage of the assets. A relevant geotechnical investigation usually require in-situ measurements and sampling of the geotechnical materials, laboratory tests, and analysis, modeling and interpretation of such data, to predict the likely future behavior of the asset.

Remote sensing based methods may have the characteristics (e. g. synoptic in nature and spatially extensive in coverage) to provide an intermediate, tradeoff level (semi-quantitative) of information between simple visual inspections, and the more expensive, detailed geotechnical analysis described in the previous paragraph. Examples of the application of remote sensing techniques to geotechnical problems are numerous, but with few exceptions (e. g. Duffel and Rudrum, 2005) they don't focus on how the obtained products can be integrated with the

geotechnical asset management. Here we propose that surface displacement derived from remotely sensed data can be used as a quantitative indicator of the performance and state of health of a series of geotechnical assets.

3. Remote Sensing Techniques and Possible Platforms

3.1 Synthetic Aperture Radar

Introduction to Synthetic Aperture Radar

Synthetic Aperture Radar (SAR) techniques have become a popular method in the remote sensing and geodesy worlds for creating digital elevation models (DEMs) and ground deformation maps. SAR data are usually obtained from antennas on a moving platform – e.g., satellite, aircraft, train, etc. – although ground-based SAR usage has become more widespread of late; this study deals with SAR data obtained via satellite platforms. The “synthetic” part of the name comes from the fact that the orbiting satellite creates a wide aperture that simulates a larger antenna. Since radar waves are transmitted and received by sensors located on the same platform on the satellite, and since radar wave transmission and reception takes time (albeit, a relatively short amount of time), the distance traversed by the satellite between transmission and reception of all radar waves that reach a given target is equivalent to the synthetic aperture length (Figure 1). If T is the amount of time a target is viewable, or within a ground swath width, from the spacecraft and c is the velocity of the radar waves (speed of light), then the length L of the synthetic aperture is:

$$L = Tc$$

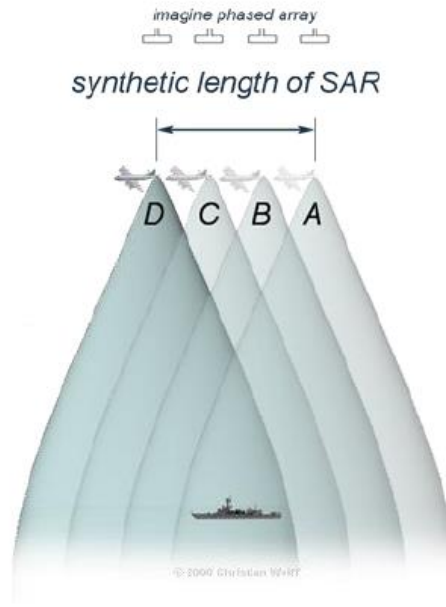


Figure 1: The length of the synthetic aperture is equal to the total flight distance where a single target is incorporated within the swath width. In this example, a synthetic aperture radar system is attached to the back of an aircraft and the target is a battleship. The battleship is viewable (within the ground swath width) of four different transmission locations (A, B, C, and D). Therefore, the synthetic aperture length (L) is equal to the distance between transmission location A and transmission location D. (Figure taken from Wolff, 2008.)

The radar echo – the radar return from the target – is received and electronically stored as a complex number in the form of:

$$Ae^{i\phi} = A \cos \phi + iA \sin \phi$$

where A is the amplitude of the radar echo and ϕ is the phase of the corresponding ground resolution cell (pixel). For sinusoidal waves, the phase is modulo 2π .

The following steps describe radar wave transmission and reception, beginning with how radar waves are emitted from the antenna, then the different types of radar reflection and backscatter that occur, and finally how targets are differentiated using information contained in the radar echo.

Step 1: Radar wave transmission (Figure 2). The satellite transmits radar waves in the range direction (perpendicular to the flight path). For the satellites used in this study, the radar waves cover a 100 kilometer-wide ground swath, with an incidence angle of 23° at the center of the

swath. The radar waves are actually emitted as short pulses (or chirps) with a center frequency of 5.331 GHz (Desnos et al., 2010). There are two major benefits for transmitting radar chirps instead of true sinusoidal waveforms: (1) a high resolution is maintained in the range direction while using a lower peak-power, and (2) it allows for azimuth compression (the azimuth direction is parallel to the flight direction), which is described in more detail in Step 3 (Dzurisin & Lu, 2007).

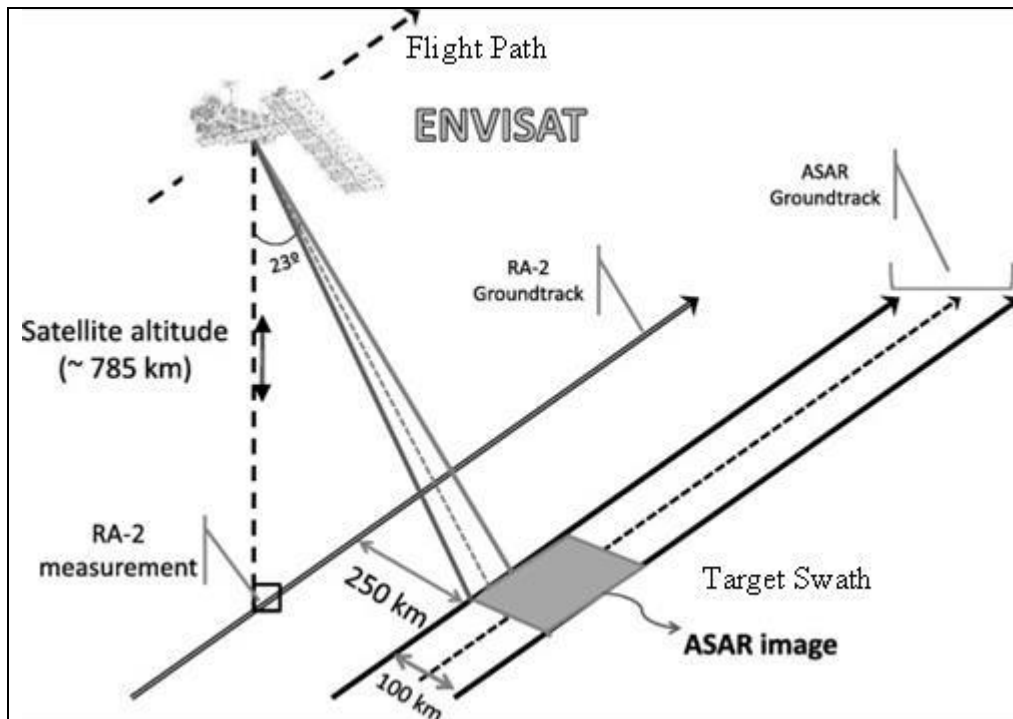


Figure 2: The flight geometry of the three satellites used in this study. The ENVISAT satellite is shown here (ESA, 2002a).

Step 2: The transmitted radar wave eventually reflects or scatters off targets in the ground swath width. The type of radar backscatter depends upon three variables: (1) the transmitted radar wavelength (5.6 centimeters for the satellites used in this study), (2) the size and shape of the targets within each resolution cell, and (3) the moisture content of the targets (Dubois, 1995). The amplitude is directly proportional to the amount of radar backscatter. In radar amplitude images, bright (or white) areas are regions of high backscatter, while dark (or black) areas indicate regions of low to no backscatter (Askne et al., 1997).

There are five types of radar wave backscatter (Freeman & Wong, 1996): (1) specular reflection – complete reflection of all incoming radar waves, similar to mirror-like reflection, appearing dark in radar amplitude images (Figure 3A); (2) volumetric scattering – geometrically complex areas, such as forest canopies, cause random scattering of radar waves in three-dimensional space, appearing variable gray in radar amplitude images (Figure 3B); (3) surface scattering – short vegetation, such as cropland, or a rough surface will result in random scattering, to a lesser extent than volumetric scattering, appearing variable gray in radar amplitude images (Figure 3C and 3E); (4) single bounce – the geometry of the target is oriented perpendicular to the incidence angle so that the reflection angle equals the incidence angle, appearing bright in radar amplitude images (Figure 3D); (5) double bounce – the geometry of the target is such that two perpendicular surfaces (e.g., a building and sidewalk) will cause the radar wave to reflect twice prior to returning, appearing bright in radar amplitude images (Figure 3F).

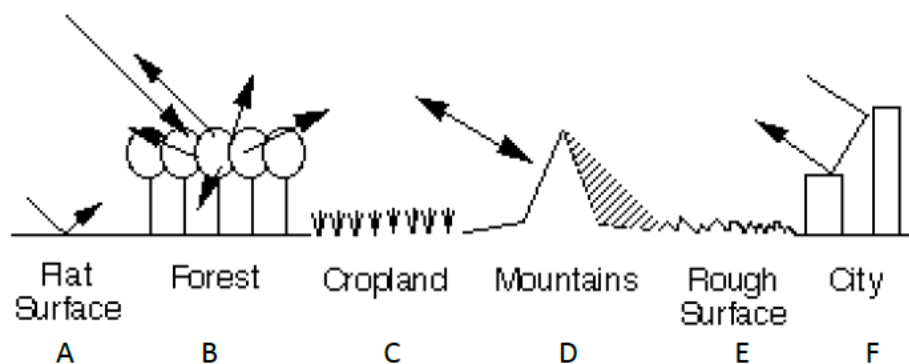


Figure 3: The types of radar backscatter: (A) specular reflection, (B) volumetric scattering, (C) surface scattering, (D) single bounce, (E) surface scattering, and (F) double bounce. (Image taken from Freeman & Wong, 1996.)

Radar backscatter signatures can become incredibly complex within one resolution cell (e.g., 625 square meters for the satellites used in this study) because there usually are multiple scattering sources (targets) that all contribute to the overall radar echo amplitude and phase. For example, a forest usually exhibits three types of backscatter. A portion of the incoming radar wave will reflect off the surface of the tree canopy (surface scattering), another portion will reflect multiple times between the branches and leaves within the canopy (volumetric scattering), and the

remaining will either single bounce off the ground or double bounce off the tree trunks and the ground.

Step 3: The radar echoes are then received by a sensor mounted on the satellite and stored electronically as a single-look complex (SLC) image. A raw (unprocessed) SLC image is composed of pixel pairs that contain both amplitude (in-phase or real component) and phase (quadrature or imaginary component) information from each ground resolution cell. A process called azimuth compression utilizes information obtained via the Doppler Effect, allowing for the ability to distinguish many more targets within a ground resolution cell (Dzurisin & Lu, 2007).

The SAR technique allows for better resolution in the azimuth direction when compared to real aperture radar (RAR), which utilizes the actual length of the antenna as opposed to a synthetically-derived antenna length. Azimuth resolution is improved by three orders of magnitude when using SAR, from the kilometer-scale with RAR to the meter-scale with SAR. The most surprising fact is the SAR resolution only depends on the real, not synthetic, antenna length (e.g., ENVISAT antenna length is 10 meters) and is not dependent on antenna distance!

SAR applications only use the amplitude portion of the received radar waves. Amplitude, or intensity ($I = A^2$), may be useful for analyzing types of features and/or backscatter mechanisms within a study area. Therefore, the major difference between SAR and Interferometric SAR (InSAR), which is basically applying SAR techniques to study temporal changes, is that the prior uses amplitude information from one acquisition while the latter mostly uses phase information obtained over multiple acquisitions (Kampes et al., 2003).

Introduction to Interferometric SAR

Interferometric SAR (InSAR) requires multiple acquisitions, all with identical radar properties (e.g., frequency/wavelength, bandwidth, etc.) and look geometry (e.g., incidence angle, line-of-sight direction, ground swath width, etc.). There are multiple techniques within the InSAR umbrella. Choosing which InSAR technique to use depends on two things: the number of acquisition images available and the purpose of the study. For example, the creation of an

optimal DEM would require just two acquisition images taken with a short period of time elapsed between acquisitions. So using a tandem image pair from the ERS-1 and ERS-2 satellites (taken one day apart back in 1995 and 1996) would be a good choice because change in topography (e.g., ground deformation) would be at a minimum and a more accurate topographic recreation would be possible. On the other hand, if the goal was to observe slow rates of movement, such as land subsidence on the scale of a few millimeters per year, two images would be insufficient. Here, a stack of radar images spanning multiple years would be the best approach because the long timespan is required to adequately measure these low ground velocities and image stacking amplifies signal while reducing noise.

There are two basic categories of InSAR techniques. The first category can be referred to as “n-pass InSAR,” where n is the number of acquisition images used in processing (n = 2, 3, or 4). 2-pass InSAR requires one master (reference) image and one slave image; 3-pass InSAR requires one master image and two slave images; 4-pass InSAR requires one master image and three slave images. n-pass InSAR is used for DEM creation or the monitoring of events over a short period of time (e.g., earthquakes, volcanic eruptions, ocean wave action, etc. – Massonnet et al., 1993; Massonnet et al., 1995). The second category can be referred to as “interferometric stacking,” where a stack of acquisition images, usually >20 images, are used to measure long-term events (e.g., subsidence, ice flow, motion of tectonic plates). Two types of interferometric stacking – persistent scatterer interferometry (PSI) and distributed scatterer interferometry (DSI) – are the methods of choice for this study.

The phase component is critical for the application of InSAR. A phase change, or phase shift ($\Delta\phi$), may be measured between a master image and a slave image. Knowing the phase shift allows for the calculation of the change in distance (Δd) between the satellite and the target over a period of time between two acquisitions:

$$\Delta d = \frac{1}{2}\lambda \left(\frac{\Delta\phi}{2\pi} \right)$$

where λ is the radar wavelength, the $\frac{1}{2}$ term compensates for the two-way travel of the radar wave, and the $(\Delta\phi / 2\pi)$ term is modulo 2π characteristic of the phase shift. As stated previously, the phase is the complex component of an SLC radar image. The phase is a measure of the location along the sinusoidal waveform – the phase shift measures the difference in the received

radar sinusoidal location along the waveform (Figure 4). A phase shift measured between two radar images acquired from the same orbital location at different times is proportional to a change in distance between the satellite and target. One radar wavelength is equivalent to a phase shift of 2π . However, if $\Delta d > (1/2*\lambda)$ between two acquisition images, the target will appear decorrelated, no information is gained. This is due to the modulo- 2π nature of the phase: if the phase shift between two images is greater than 2π (one full rotation), we are unable to calculate how many rotations occurred; for example, $\Delta\phi = \pi = 3\pi = 5\pi = (n+1)\pi$ (if n is an even integer ≥ 0). Therefore, $\Delta\phi \leq 2\pi$ must be true or else decorrelation will occur. This means the maximum displacement (Δd_{max}) that can occur without decorrelation is:

$$\Delta d_{max} = \frac{\lambda}{2}$$

...because if, for example, a target on the ground moves a distance of $(\lambda/2)$ away from the satellite, the transmitted radar wave must travel that distance *twice*, and that corresponds to a total distance of λ , which is equivalent to a 2π phase shift.

There are a few ways to avoid this decorrelation problem. The first would be to obtain a temporally dense set of acquisition images. Decorrelation due to excess displacement will not occur so long as $\Delta d \leq (\lambda/2)$ between each acquisition. If a dense stack of images is not possible, another solution would be to find a satellite with a longer wavelength. This would increase the amount of allowable displacement between acquisition images. And if neither of these two solutions is possible, then one must search for a less active study area.

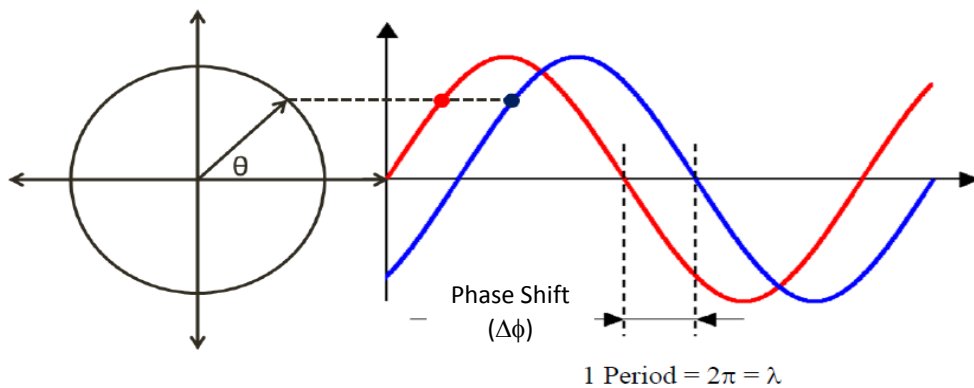


Figure 4: A visual representation of the phase (θ) and the phase shift ($\Delta\phi$) for two different acquisitions. The two incoming radar waves are offset and thus a phase shift is measurable.

Generation of SAR Products

Prior to discussing the specifics to interferometric stacking, the general InSAR processing steps are explained. All InSAR processing, regardless if the technique is n-pass InSAR or interferometric stacking, requires the completion of the seven-step workflow described in the “General InSAR Processing Steps (1-7)” section below. The only difference between n-pass InSAR and interferometric stacking is the number of acquisition scenes that are processed through the workflow. The next two sections – “Persistent Scatterer Interferometry” and “Distributed Scatterer Interferometry” – each discusses additional processing that is incorporated within that technique to obtain results.

General InSAR Processing Steps (1-7)

There are seven general InSAR processing steps that must be performed to convert SLC slant-range image data to line-of-sight (LOS) ground displacements. The seven steps are: (1) baseline estimation, (2) interferogram generation, (3) coherence and adaptive filtering, (4) phase unwrapping, (5) orbital refinement, (6) phase to height conversion and geocoding, and (7) phase to displacement conversion.

Step 1: Baseline Estimation. Knowing the exact location of the satellite along its orbital path at each pass is incredibly important (this point will be further elaborated on in Step 7). Ideally, the satellite would be in the exact same location every time it passed over a target. Unfortunately, this is not the case. The perpendicular baseline (B_{\perp}) is the distance, in the direction perpendicular to the flight direction, between satellite locations at different acquisitions over the same target (Figure 5). The baseline estimation is important because if $B_{\perp} > 1,000$ meters (the critical baseline for the satellites used in this study), then there is a loss of coherence between the acquisition pair because the radar viewing angles are too different and, therefore, a loss of InSAR capabilities (ESA, 2008).

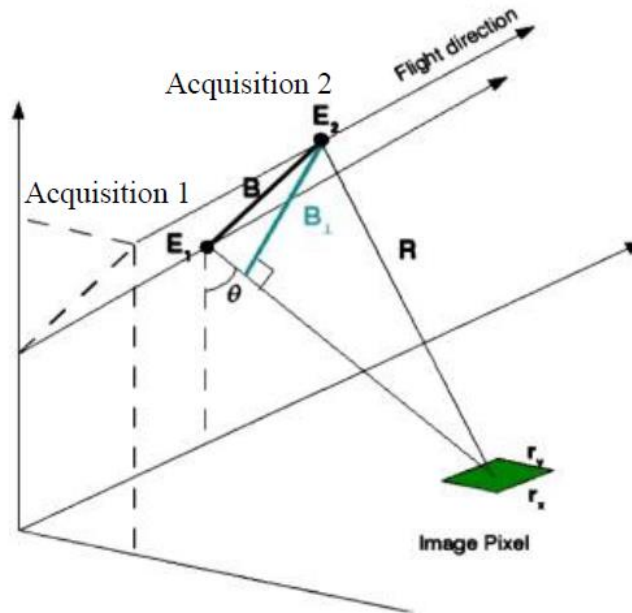


Figure 5: Schematic of two different acquisitions (E_1 and E_2) of an orbiting satellite. Notice the difference in baseline (B) and perpendicular baseline (B_{\perp}). An acquisition pair is usable as long as $B_{\perp} <$ critical baseline (1,000 meters for satellites used in this study). θ is the incidence angle and R is the range distance between the satellite and the target resolution cell (image pixel) with dimensions r_x and r_y . (Image taken from Ahmed et al., 2011.)

Step 2: Interferogram Generation. This step actually incorporates five sub-steps (Hooper et al., 2004): (1) image co-registration, (2) complex interferogram generation, (3) spectral shift and common Doppler filtering, (4) interferogram generation (includes topography), and (5) interferogram generation (excludes topography).

(1) *Image Co-Registration* – This is the process of spatially aligning more than two images so that geographic identical pixels are placed in the same location (eventually by latitude, longitude).

(2) *Complex Interferogram Generation* – A complex interferogram is a mathematical product equal to the coherence of the master image and the complex conjugate of the coherence of a slave image (Ferretti et al., 2000). The result is a fringe pattern image that contains all the information on the slant-range geometry of the study area (Ferretti et al., 2001).

(3) *Spectral Shift and Common Doppler Filtering* – These are applied to the received radar signal that has undergone a spectral shift (usually due to a change in radar wave velocity

between transmission and reception). The spectral shift and common Doppler filtering calculate and tune the filters to these changes in center frequency (Bamler & Hartl, 1998).

(4) *Interferogram Generation (Includes Topography)* – An interferogram is created using a pre-defined ellipsoid as the datum. This is usually referred to as the ‘synthetic interferogram,’ as the fringes within an interferogram still (at least) contain topographic and atmospheric information (Ferretti et al, 2000).

(5) *Interferogram Generation (Excludes Topography)* – An interferogram is created using the synthetic interferogram (from the previous sub-step) and a DEM. This allows for the subtraction of topographic information from the interferometric fringes, leaving sources for phase change as atmospheric phase delay, ground deformation, and systematic noise (Ferretti et al, 2001).

Step 3: Coherence and Adaptive Filtering. The coherence (γ) between two co-registered SAR images (master and slave) is defined as the ratio between the summation of the coherent and incoherent radar data:

$$\gamma = \frac{|\sum s_1(x) \cdot s_2(x)^*|}{\sqrt{\sum |s_1(x)|^2 \cdot |s_2(x)|^2}}$$

...where $s_1(x)$ and $s_2(x)$ are the coherence images from the master and slave acquisitions, respectively, and $s_2(x)^*$ is the complex conjugate of the coherence file (Ferretti et al., 2000). Coherence values range from 0 (incoherence or pure noise) to 1 (all signal, no noise), and is a function of systemic spatial decorrelation, natural scene decorrelation, and additive noise (Askne et al., 1999).

Adaptive filtering eliminates pixels that exhibit high noise (low coherence) from the interferogram generated in Step 2(5) (Lopes et al., 1993). The coherence threshold, a user-defined variable, is used to eliminate all pixels with coherence below the coherence threshold.

Step 4: Phase Unwrapping. This is the process that resolves the 2π ambiguity of the interferogram data. Phase unwrapping basically ‘translates’ the wrapped phase values into absolute phase values (Figure 6). What is meant by the word ‘translates’? The phase of the incoming radar wave quantifies the wavelength location, or in other words, it records at what point along the wavelength the radar wave is received by the sensor. Each point along the wavelength is assigned a phase number, ranging from 0 to 2π . If the phase number increases above 2π , it is reassigned a value between 0 and 2π , and is therefore considered ‘wrapped.’

Unwrapping the phase allows for a phase ramp of continuous values, which is beneficial when calculating the distance between the satellite and pixels within the target area.

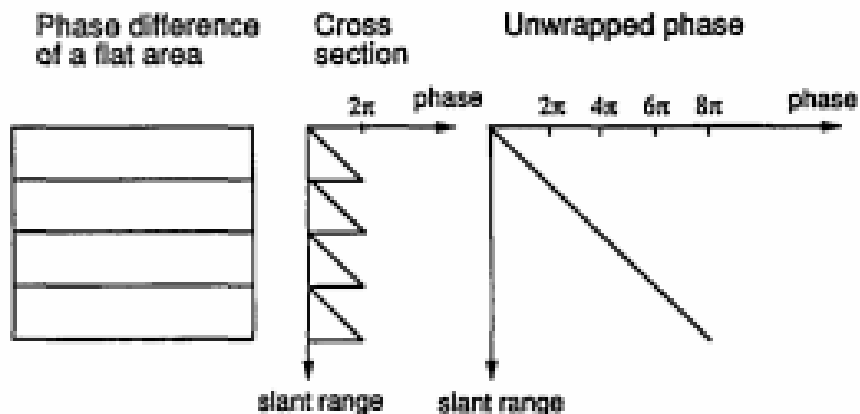


Figure 6: If each of the segmented rectangles on the left illustrate fringe lines, the cross-section in the middle shows the associated phase values. Phase jumps – the instantaneous change in phase value from 2π to 0 – create the saw-tooth-shaped cross-section; this is the wrapped phase. By eliminating the confines of the phase, the unwrapped phase can be displayed continuously, with respect to slant range, as shown on the right; this is the unwrapped phase. (Image taken from Lin et al., 1994.)

Step 5: Orbital Refinement. This procedure makes it possible to calculate the absolute phase and the phase offset between acquisitions, to refine the satellite orbit, and to reduce the corresponding perpendicular baselines. Orbital refinement accounts for the shift in azimuth (flight direction) and range (perpendicular to flight direction) directions, the spatial convergence of the orbits in both directions, and the absolute phase (Kohlhase et al., 2003).

Step 6: Phase to Height Conversion and Geocoding. The absolute phase for each acquisition pair (master and slave) is converted to height values for each image pixel. Each pixel height contains precision and error information (Bayer et al., 1991). The image is then geocoded into a user-specified map projection.

Step 7: Phase to Displacement Generation. Phase shifts between multiple acquisitions are influenced by as many as five variables, shown in the following equation (Hooper et al., 2004):

$$\Delta\phi_{int} = \Delta\phi_{topo} + \Delta\phi_{sat} + \Delta\phi_{disp} + \Delta\phi_{atm} + \Delta\phi_{noise}$$

...where the total phase shift in the interferogram ($\Delta\phi_{int}$) is the sum of the phase shifts due to the topography ($\Delta\phi_{topo}$), the change in satellite position ($\Delta\phi_{sat}$), ground motion ($\Delta\phi_{disp}$), all atmospheric phase delay effects ($\Delta\phi_{atm}$), and additive or systemic noise ($\Delta\phi_{noise}$). The purpose of

some of the previous steps was to eliminate phase shifts due to extraneous factors: Step 3 reduces the $\Delta\phi_{\text{topo}}$ phase shift component; Step 3 reduces the $\Delta\phi_{\text{noise}}$ component; Step 5 reduces the $\Delta\phi_{\text{sat}}$ component. Two phase shift components remain: $\Delta\phi_{\text{atm}}$ and $\Delta\phi_{\text{disp}}$.

In order to separate the phase shift due to ground displacement and the phase shift due to atmospheric effects, one of two approaches can be taken. The first approach is to obtain atmospheric data (e.g., water vapor content products from the Medium Resolution Imaging Spectrometer (MERIS) instrument on the ENVISAT satellite), which can be used as an input into an atmosphere-reduction pre-processing step (ESA, 2013). The second approach is to make an assumption: that the atmosphere does not vary enough laterally to warrant the need to remove these effects. Most programs (including SARscape) already apply atmospheric filters. Atmospheric effects can be avoided by choosing images acquired on days without precipitation events and by processing over a small area, where lateral atmospheric changes are less likely.

Persistent Scatterer Interferometry

One of the two interferometric stacking techniques used in this study is Persistent Scatterer Interferometry (PSI). The PSI processing procedure incorporates all of the processing steps described above, but the output differs. This technique searches the input radar images for pixels with consistently high coherence throughout a stack of 20 images or more. A pixel with consistent coherence usually exhibits a relatively stable geometry (no spatial or temporal decorrelation) and a surface that allows for a great amount of radar backscatter to return to the satellite sensor (echo). Targets that generally fulfill these requirements are usually anthropogenic structures, such as roads, bridges, buildings, and dams. They may also be natural features, such as rock outcrops or cliff faces that lack vegetation. Targets with consistently high radar returns are known as persistent scatterers (PS) and are the only points with ground displacement information in the PSI output. All other non-PS pixels are discarded and provide no information (Ferretti et al., 2000; Ferretti et al., 2001).

The interferometric stacking rule-of-thumb is the slower the ground deformation (e.g., sediment compaction that occurs on the millimeter/year-scale), the longer the period of time needed to measure the deformation (Hooper et al., 2004; Bürgmann et al., 2006). This introduces a problem regarding coherence: if a long time is needed to measure the ground motion, then it is more

likely that the targets will lose coherence. Since PSI requires pixels with consistently high coherence over the timespan of the study, the way to work around this problem is to obtain as many radar images as possible within the time of interest. This coherence problem is the main reason why a stack of radar images is required for this technique.

Similar to any other radar interferometric technique, PSI has its advantages and limitations. Advantages of using PSI include: (1) the ability to cover urban areas with high PS density (thousands of PS/square kilometer); (2) the ability to detect millimeter/year-scale ground velocities; and (3) the vast historical archive of data from sources such as the European Space Agency, the National Aeronautics and Space Administration, the Canadian Space Agency, and the Alaska Satellite Facility. Limitations of PSI include: (1) the inability to measure relatively quick ground deformations (e.g., greater than 2.8 centimeters between acquisition); (2) PS locations are unknown prior to processing; (3) all ground deformation measurements are made in the line-of-sight (LOS) direction; and (4) there exists an extreme variable spatial sampling, where urban areas yield a high PS density while rural and vegetated regions yield a low PS density (less than 50 PS/kilometer) (Crosetto et al., 2010).

Distributed Scatterer Interferometry

The second interferometric stacking technique used in this study is Distributed Scatterer Interferometry (DSI). DSI addresses the fourth limitation of PSI (addressed in the previous section), which is that the PSI technique may yield thousands of PS/kilometer in urban areas, but only tens of PS/kilometer in rural or vegetated areas. Using DSI, we are able to locate distributed scatterers (DS) that give us exactly the same information that PS do (e.g., ground velocity), but DSI is applicable in rural and vegetated regions.

There are many algorithms that search for DS. The algorithm used for this study is SqueeSAR™ and was created by Tele-Rilevamento Europa (TRE), an advanced InSAR technologies company based out of Italy and Canada. The SqueeSAR™ algorithm can be described in the following six steps (Ferretti et al., 2011):

1. The DespeckKS algorithm (which basically stands for Despeckle Kolmogorov-Smirnov) is used to identify the family of statistically homogeneous pixels (SHPs) for each pixel (P). SHPs are groups of adjacent pixels that exhibit similar radar returns. Let N_s be the number of SHPs.

2. For those SHP groupings where N_s is greater than a user-defined threshold, they will be defined as DS.
3. For all DS, a sample coherence estimation is performed with the specific information gained from Step 1.
4. A phase triangulation algorithm (PTA) is applied across each coherence matrix from each DS.
5. All DS with a PTA value greater than another user-defined threshold will substitute the original phase values with optimized phase values.
6. Last, the DS are processed jointly with the PS (from the PSI technique). A time-series with both DS and PS is generated.

DSI, and SqueeSAR™ specifically, allows for better coverage across rural and vegetated regions, where PSI inherently fails. The result is a greater density of PS-DS points across the study area. One idea must be kept in mind when interpreting DSI data: the PS points contain information only from one pixel, while DS points contain information from a group of N_s -sized pixels surrounding the displayed DS.

Satellite Platform Specifications and Products

Radar images from four satellites – ERS-1, ERS-2, ENVISAT, and RADARSAT-1 – are used for this study. Table 1 lists and compares the technical and acquisition parameters for each satellite (ESA, 2002b; ESA, 2012).

Table 1: InSAR satellite and sensor characteristics.

Parameter	ERS-1	ERS-2	ENVISAT	RADARSAT-1
Orbit Type	Near-Circular, Polar, Sun-synchronous	Near-Circular, Polar, Sun-synchronous	Near-Circular, Polar, Sun-synchronous	Near-Circular, Polar, Sun-synchronous
Acquisition Dates	1991-2000	1995-2011*	2002-2012	1995-2008
Altitude (km)	782-785	782-785	772-774	793-821
Inclination	98.52°	98.52°	98.40°	98.60°
Period (min)	~100	~100	~100	~100
Orbits/day	14.3	14.3	14.3	14.3
Repeat Cycle (days)	35	35	35	35
SAR Instrument(s)	Active Microwave Instrument comprising a SAR (image/wave) modes; Radar Altimeter	Active Microwave Instrument comprising a SAR (image/wave) modes; Radar Altimeter	Advanced Synthetic Aperture Radar (ASAR); Radar Altimeter 2 (RA-2)	Standard Beam SAR (Fine Beam SAR)
Incidence Angle	23°	23°	23°	20-49° (30-50°)
Frequency (GHz)	5.3° C-Band	5.3° C-Band	5.3° C-Band	5.3° C-Band
Wavelength (cm)	5.6	5.6	5.6	5.6
Polarization	VV	VV	VV	VV
Spatial Resolution (m)	30	30	30	30 (~8)
Swath Width (km)	100	100	100	100 (50)

*ERS-2 had some gyroscopic malfunctions in February 2001 – data is unreliable after that point (ESA, 2008).

3.2 LiDAR

Lidar is an active form of remote sensing. Active means that the LiDAR sensor is generating energy that is used to create the remote sensing data. The light pulse flies from the laser till it hits an object, and then the reflected laser light is recorded by another telescope to determine the time of flight of the laser energy. The time of flight is used to calculate the distance from the LiDAR sensor to the feature, in our case being the ground or slope.

The platform on which the LiDAR sensor is mounted can be stationary or mobile. Mobile platforms can be vehicles on the ground or aircraft, and even spacecraft. Stationary LiDAR sensors are typically mounted on survey tripods.

On all platforms, the LiDAR sensor is coupled with other sensors to record the LiDAR sensor's position. With mobile platforms, other sensors record its orientation. Position is recorded using a global navigation satellite system (GNSS). An inertial navigation system (INS) records the motion and orientation of the truck or aircraft as it drives or flies (figure 7).

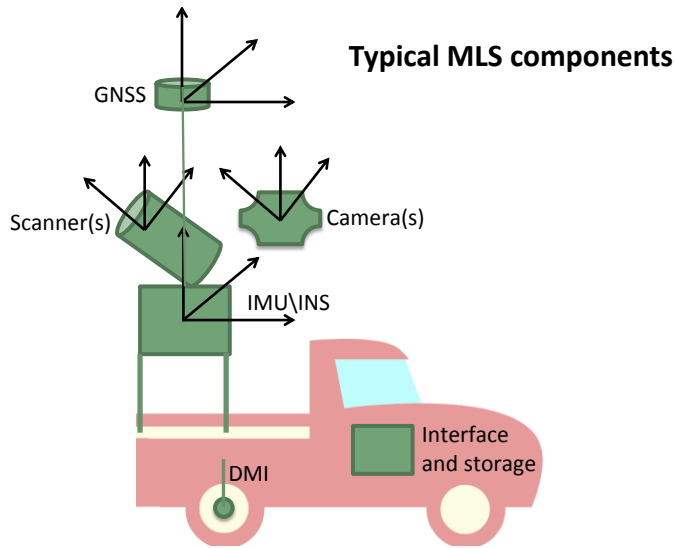


Figure 7 Components of a mobile LiDAR system (from NCHRP Report 748)

The distance of the LiDAR sensor from the feature being imaged determines the density and resolution of the LiDAR data being collected. Close range laser scanning collects dense, high-resolution data. Aircraft mounted LiDAR sensors collect relatively sparse data, but over much larger areas with great efficiency, compared to static terrestrial LiDAR scanners (figure 8). As with other remote sensing technology, LiDAR has seen increases in data collection rates and more dense data sets.

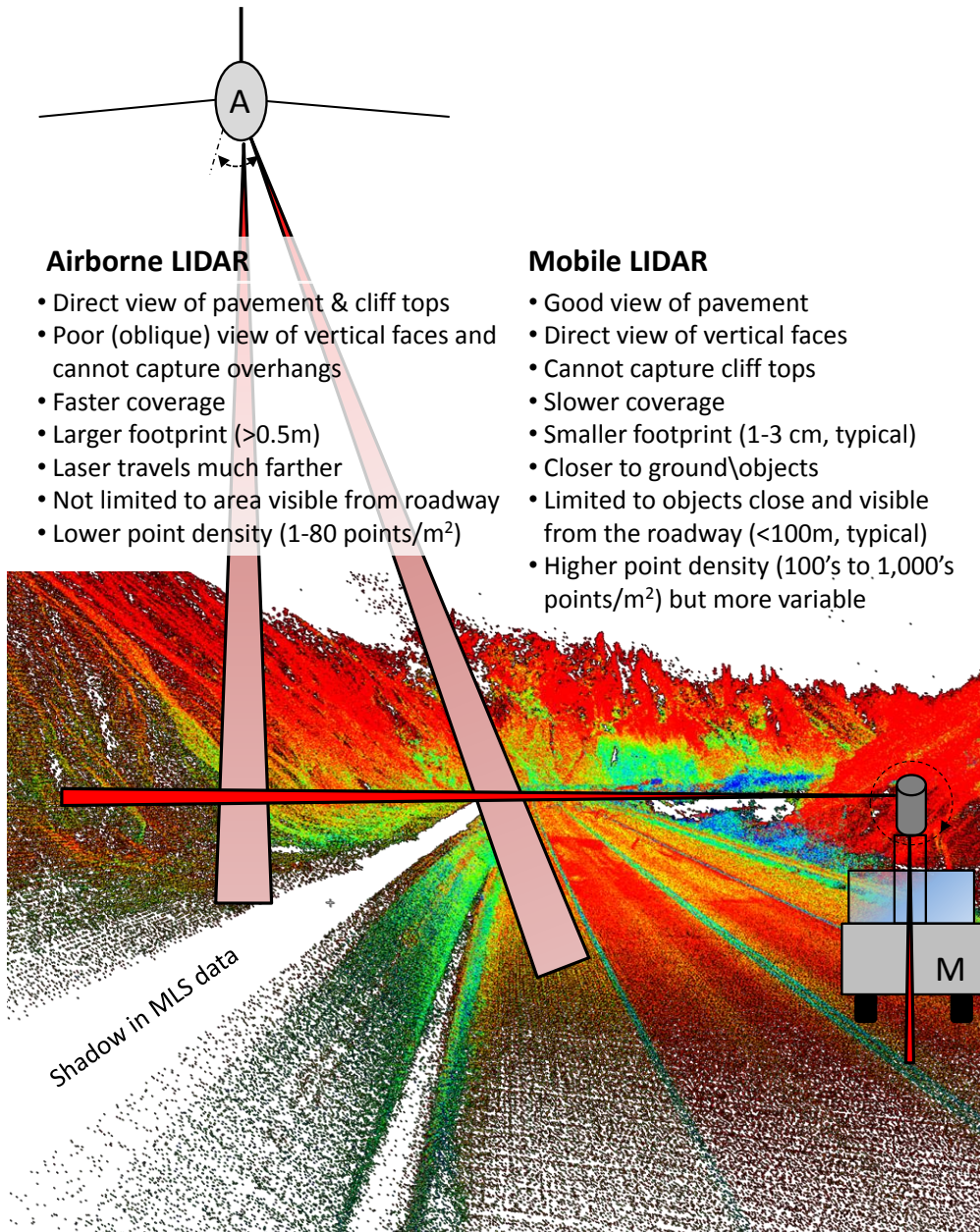


Figure 8 Comparison of airborne and terrestrial mobile LiDAR systems at Glitter Gulch project site (from *A Platform for Proactive, Risk-Based Slope Asset Management, Phase II*, by Cunningham, Olsen Wartman and Dunham).

The LiDAR data collected is often described as a point cloud. The point cloud has three-dimensional position measurements for the features being scanned. Besides the features of interest on slope, there are other types of data in the point cloud, such as cars on a road, people on a sidewalk, houses, trees, and even the branches and leaves on a tree. To make the LiDAR data in the point cloud useful, the data must be processed and filtered (figure 9). Many LiDAR

vendors provide processing data, however third-party software is usually required for the filtering of data to derive various LiDAR data products.

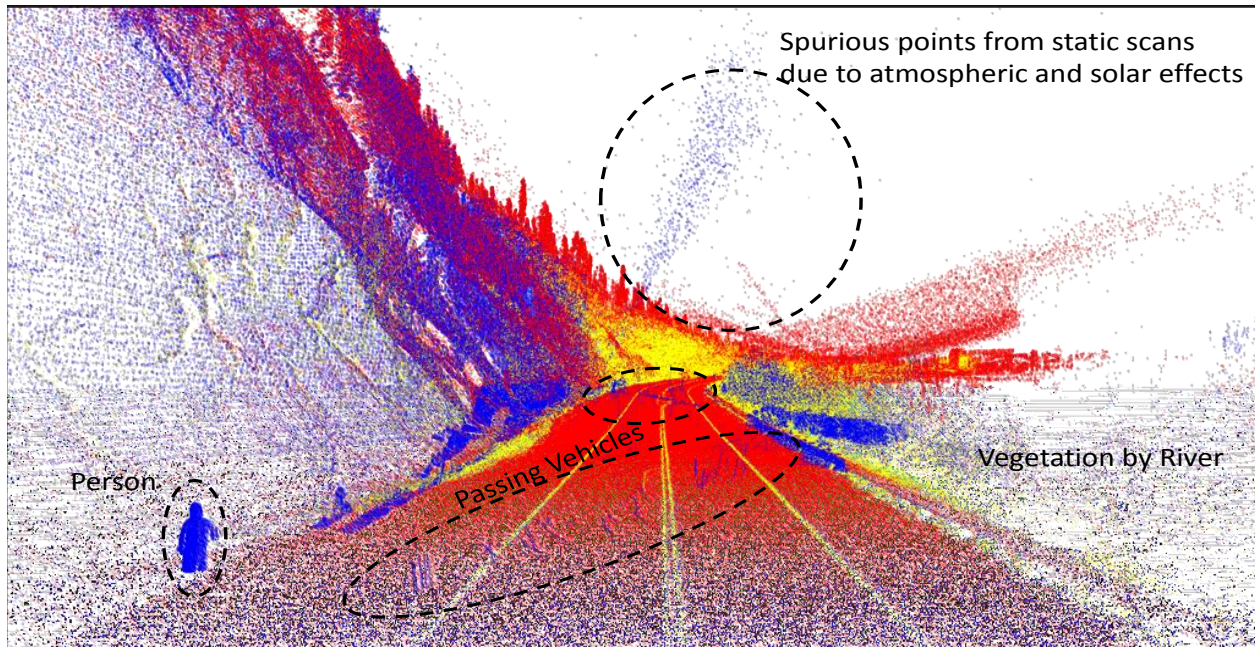


Figure 9. Lidar point cloud with examples of noise to be filtered and removed at Glitter Gulch project site (from A Platform for Proactive, Risk-Based Slope Asset Management, Phase II, by Cunningham, Olsen and Wartman).

Filtering airborne data is performed by looking down at the data from the perspective of the aircraft – and these filtering algorithms were some of the very first developed to remove features above the ground in order to extract a bare earth data set. Filtering terrestrial data, from a moving vehicle or a static tripod is more involved because the filtering algorithms are not mature for the various applications that the LiDAR data can be used. For geotechnical analysis, it is typical to remove vegetation in order to measure the bare earth (figure 10).

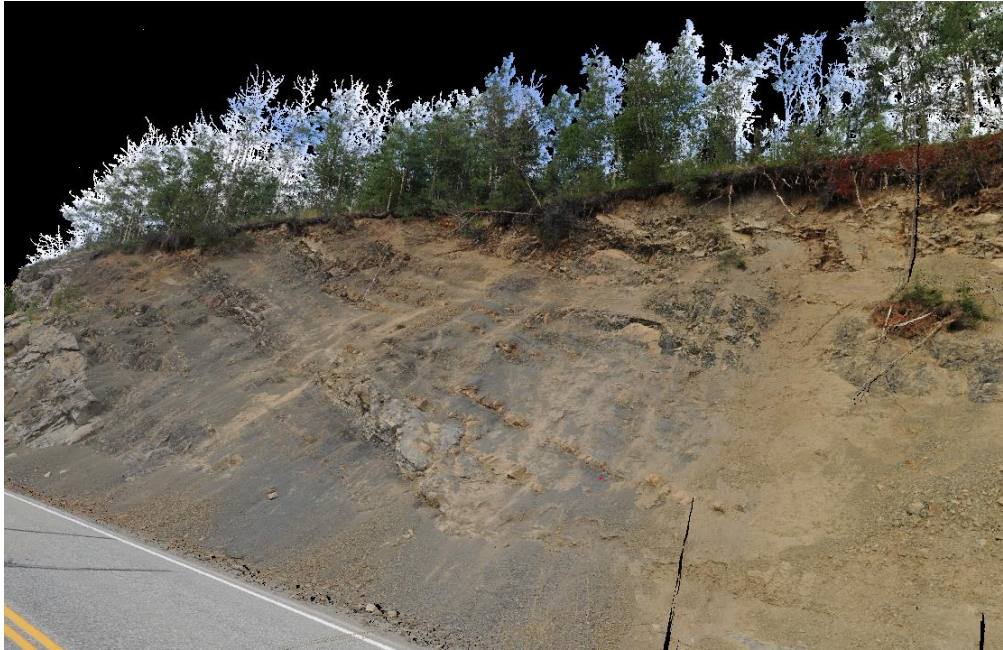


Figure 10. RGB colorized LiDAR point cloud at the Glitter Gulch project site (from [A Platform for Proactive, Risk-Based Slope Asset Management, Phase II](#), by Cunningham, Olsen and Wartman).

One LiDAR scan can be used as a base line measurement. Subsequent LiDAR scans can then be compared to the baseline to analyze the data for change. Examples of change detection in geotechnical engineering are the erosion and accretion of talus on highway road cut slope. Lidar change detection also measures and monitors displacements and deformations in retaining walls, dams, and other man-built features. The different LiDAR data sets must be carefully co-registered in order to make an analysis of change. This technique subtracts one LiDAR data set from the other to report the difference. The differences are then visualized creating a graphic showing the deformation or displacement.

Accuracy and precision of the LiDAR scan data vary with the LiDAR system and its platform. Airborne LiDAR accuracies are typically measured in decimeters (feet) with precisions on the order of 15 centimeters (0.5 foot). Terrestrial LiDAR on tripods are much closer to the features being scanned and they are accurate to a few centimeters, which is also the precision of the measurement. Thus distance of the LiDAR scans affect accuracy, largely because of the humidity and temperature of the atmosphere that attenuates and diffracts the laser energy as it passes through the air. Also, the GNSS, and INS referencing affect the accuracy of the LiDAR

data. It is important to note that INS are especially susceptible to a type of error called drift, which adds a cumulative error until the drift is corrected in a calibration process after the data is collected.

3.3 Optical Photogrammetry

Optical remote sensing is most commonly done by using sensors that are sensitive to the visible portion of the electromagnetic spectrum. This corresponds to wavelengths of light are between 400 and 700 nm. Optical systems are able to detect near infrared (IR) wavelengths of light (approximately 700 to 1300 nm or 1.3 microns) but use filters to prevent them from being detected by the sensor; however, digital cameras can have their filter removed. The most common optical sensors are Charge-Coupled Devices (CCDs), which are used in typical consumer-grade digital cameras. The wide scale availability of digital cameras and low cost make them a good candidate for characterizing remote sensing applications. These sensors have been developed to be smaller as they are used for cell phone cameras as well as in professional photography.

Photogrammetry is “the science or art of deducing the physical dimensions of objects from measurements on photographs of the objects” (Henriksen 1994). This includes measurements made from both film and digital photography. Digital photogrammetry has been demonstrated as a viable technique for generating 3D models of structures and structural elements (Maas and Hampel 2006). In order to perform 3D photogrammetry, the photos need to be taken with at least a 60% overlap (McGlone et al. 2004). This ensures that a feature on the ground is represented in at least two photos, as illustrated in Figure 11. At distances closer to the surface than traditional aerial imagery this technique is more specifically called close-range photogrammetry. Close-range photogrammetry is defined as capturing imagery of an object or the ground from a range of less than 100 m (328 ft) (Jiang et al. 2008).

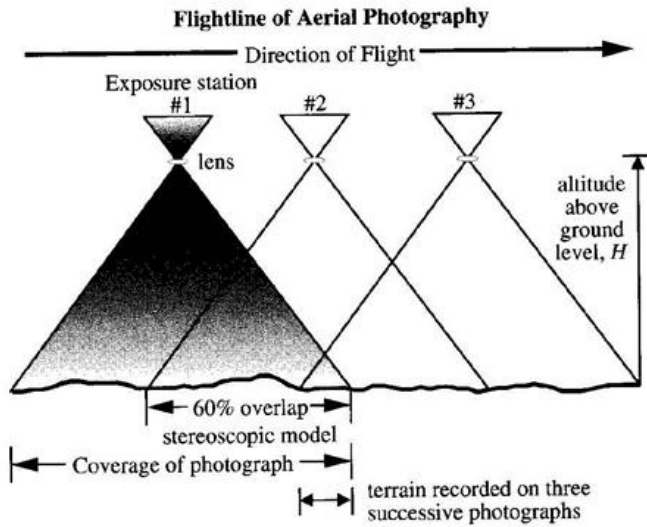


Figure 11. An example of how stereoscopic imagery for generating 3D models is collected (Jenson 2007).

Typically, 3D models are generated by using the bundle adjustment principle (Triggs et al. 2000). This process used determines the orientation of each image in a series of overlapping images to generate a sparse point cloud (Triggs et al 2000). Figure 12 shows the triangulation between multiple images that is used during this process. This process allows for images to be taken at different angles, which occurs when the camera rolls and changes pitch as it is moved across its target.

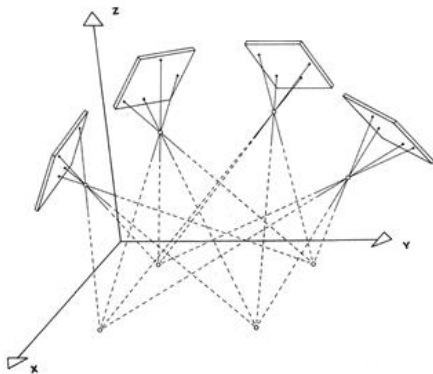


Figure 12. Bundle adjustment seeks to solve the geometry between photos and to generate 3D point clouds. This figure shows the relationship between four images that is solved by the bundle adjustment (Wester - Ebbinghaus 1988).

This technique allows for additional height information to be extracted from the imagery. With recent advances in close range photogrammetric software, the generation of DEMs is mostly

automated. Some software applications, such as Agisoft PhotoScan, only require the user to input the photos and a 3D model is generated without any further interaction. In order to generate a DEM the user has to set up a real-world projected coordinate system. This is done by placing markers with known GPS coordinates on the surface being modeled or by geo-tagging the images as they are taken. This technique was used by Ahlborn et al. (2013) to locate spalls on bridge decks with a truck-mounted camera and also by Brooks et al. (2013) to characterize distresses on an unpaved road.

4. Requirements of remote sensing techniques for geotechnical asset management for regional scale condition assessment

4.1 Synthetic Aperture Radar

The monitoring and measuring of ground deformation of geotechnical assets can be conducted using the InSAR stacking techniques discussed in Section 3.1. At the regional scale – a large network of geotechnical assets – both PSI and DSI are able to detect ground motion on the millimeter/year-scale with at least 20 radar images in a processing stack. Of course, the largest issue with stacking techniques is whether or not a sufficient number of PS and/or DS points will appear on the geotechnical assets in question. At the regional scale, we would need enough PS/DS points across the asset network. Issues that may arise when attempting to monitor an entire geotechnical asset network are listed below.

(1) The largest issue is whether or not PS/DS points will be present on the geotechnical assets within the study area. Section 5.1 discusses in great detail the likelihood of points appearing on different geotechnical assets and some causes as to why (or why not) points would be available.

(2) Depending on the overall purpose of the study, the size of the geotechnical asset network to be processed may be limited to the satellite radar swath width/area. For example, the swath width for the satellites listed in Table 1 (Section 3.1) is 100 km, resulting in a swath area of 100 km x 100 km (10,000 square kilometers). Each swath aligns with an orbital track, either in the descending (north-to-south) or ascending (south-to-north) direction. SLC radar image stacks can only be processed if all images were acquired along the same track from the same satellite. Therefore, there is a limit to the geotechnical asset network's areal extent per processing stack. If

the geotechnical asset network is not contained within one stack, additional radar images must be obtained and placed in a different stack. One important notion must be understood: two adjacent orbital tracks will contain radar images obtained from different dates and, possibly, different times (during the day). Therefore, the two stacks will *probably differ* in many temporal variables, such as the timespan, the number of images within the stack, and the frequency of images throughout the stack (e.g., one stack may have more images in 2004 while another contains more images in 2006).

(3) It is important to understand the differences in weather and climate across the geotechnical asset network. For example, let us take a geotechnical asset network where the western portion is located in a desert and the eastern portion is located in a mountainous terrain. The best conditions for radar acquisition are low atmospheric variability (e.g., little water content) and dry ground conditions. Therefore, there may not be much cause for concern for weather-related affects in the western desert region. However, the seasonal presence of snow and changes in atmospheric pressure and water vapor may have a heavy influence on radar effectiveness in the mountainous regions. So it may behoove of the investigator to obtain radar images during times of the year when the mountainous regions are not as affected by the weather.

(4) Each satellite is operated and funded by certain organizations. These organizations have areas of interest across the world. It is vitally important to check respective online databases as to whether the satellite has acquired radar images over your study area and, if so, what the timespan of these data are. Radar images are available from various agencies. The data timespan available for some satellites is astonishing. For example, the ERS-1, ERS-2, and ENVISAT radar data are all compatible and images are available (in some places) from 1992 to 2011. The European Space Agency has just launched Sentinel-1 (April 2014) and has plans to launch additional satellites in the near future – all of which are supposed to be compatible with ERS-1, ERS-2, and ENVISAT.

Please refer to Section 5.1 for issues that may arise on the local scale (one geotechnical asset) and how these issues can be resolved. It is important to understand whether PS/DS points will be resolvable at the local-scale before expanding the processing area to a regional-scale.

4.2 LiDAR

At a regional scale, defined as a large network of geotechnical assets, such as a right-of-way through mountains, only mobile LiDAR is an efficient remote sensing tool. Static terrestrial LiDAR, while superior in data density and accuracy to mobile LiDAR, is difficult and expensive to collect for areas larger than specific sites.

Mobile LiDAR includes systems mounted on aircraft (airborne) and trucks (terrestrial). Both the terrestrial and airborne mobile systems require precise synchronization and calibration with the GNSS and INS systems. Calibration requires averaging out the cumulative orientation and positioning error caused by INS drift, which increases with longer periods of data collection. Another aspect of calibration with both platforms is the need for horizontal control of the LiDAR point cloud and the final registration of the point cloud in a precise vertical coordinate system using an ellipsoid datum. When regional LiDAR is collected for updating flood plain maps, a much more accurate vertical datum is a requirement. When the most accurate vertical measurements are needed, for hydrologic and hydraulic models, an even more accurate geoid datum is necessary to understand the effect of the earth's gravity on vertical measurements in order to model the movement of water.

Both airborne and terrestrial mobile systems are also characterized by less-dense data than the static terrestrial systems collected at smaller study sites. Lidar “postings” which are the samples recorded from an aircraft can be on the order of 1.8 meters (five foot) among the ground measurements. With terrestrial vehicles, the postings can be much denser, say 10 centimeters among the samples. Regional LiDAR data postings of 1 – 2 meters enable broad-scale and long-term studies of slope stability and other geotechnical hazards such as faults and sink holes. The mobile terrestrial scans allow the inventory of geotechnical assets such as guard rails, retaining walls, and other “street furniture” found along a transportation corridor.

While the collection of airborne and terrestrial mobile LiDAR are cost effective for regional collects, repeated data collection over time is less common. This is because regional LiDAR data collection is usually for mission specific purposes such as a proposed road alignment or

flood plain mapping. These infrequent data collect limit the application of this type of LiDAR to opportunistic geotechnical studies focused on change detection.

Another limitation of regional LiDAR is the lack of detail for site-specific geotechnical features and small-scale hazard analysis, such as the movement of a retaining wall or a small talus slide.

4.3 Optical Photogrammetry

Regional scale photogrammetry would utilize aerial platforms to collect imagery of large areas. This could include the use of UAVs or manned aircraft depending on the scale and resolution required. The use of aerial vehicles allows for the rapid assessment of geotechnical assets over a large area.

Requirements for these type of data collection systems are primarily dependent upon weather conditions. Manned aircraft are typically flown under high-pressure weather systems. This usually gives way to clear skies and low wind. Also, the time of day is critical, as the sensor should be between the target and the sun. This will reduce glare in the optical image. Manned vehicles are also capable of carrying multiple sensors and are less impacted by wind conditions. When using UAV systems, weather remains the largest factor of successful data collection. UAV systems are more sensitive to wind, because of their size and engine/motor power, and are thus limited by high wind gusts. However, because a UAV will fly at a much lower altitude there is less importance on time of day as the sensor will more often lie between the target and the sun.

The type of asset being sensed must also be considered. If a clean image of a slope is needed, performing data collection during the early spring or late autumn is necessary. This will ensure that the trees do not have leaves, which would obstruct the needed imagery.

5. Requirements of remote sensing techniques for geotechnical asset management for local scale performance monitoring

5.1 Synthetic Aperture Radar

Section 4.1 discussed the regional-scale issues that may arise during PSI and DSI processing. This section lists a number of issues that may arise on the local-scale (one geotechnical asset). Once again, the number of PS and DS points available for interferometric stacking is vitally important because these points contain all ground motion information. Understanding what influences the presence of PS/DS points is important. The number of these points greatly depends on the following # variables.

(1) The topography of the area will dictate how many of the geotechnical assets are within the radar's view. For example, shadowing is an issue in mountainous terrain where only one side of a mountain will be viewable from the radar sensor while the opposite side, facing away from the sensor in the mountain's "shadow," will not provide any information. Therefore, it is critical to know the topography of the study area (e.g., are there mountains, canyons, valleys, etc. that block the sensor from key geotechnical assets?) and to understand the look direction and incidence angle of the satellite radar sensor (e.g., ENVISAT has a right-looking radar sensor inclined at $\sim 23^\circ$ from vertical).

(2) The amount of vegetation greatly influences the number of available points, more so for PS points than for DS points. If the geotechnical assets of interest are covered in vegetation, there is much less chance for success in obtaining points with ground deformation information on them. PS points require a consistently high coherence for each pixel and, with the presence of vegetation, it is entirely likely no points will be found in these regions. DS points, on the other hand, do not require strict coherence standards as PS points and, therefore, there is a chance of obtaining DS points within vegetated regions, but it is not a guarantee. Geotechnical assets with no vegetation, such as rock slopes and embankments, bare earth landslides, rock falls, bridges, etc., should be detectable using PSI and DSI.

(3) Similar to the topography issue in (1), the geometry of the geotechnical asset itself plays an important role in whether PS/DS points will be present. An additional concern here are vertical assets, such as retaining walls, because the geometry of the asset is such that it may be difficult for any radar echoes to return to the satellite. The hope for vertical assets is two-fold: (1) that the ground near the asset is relatively smooth and (2) that the vertical asset and the smooth ground are facing the satellite look direction. If both these conditions are true, there is a chance

that the incoming radar waves will double-bounce off the road and vertical asset and return to the satellite. If this is the case, then PS/DS points should be resolvable on the vertical asset.

(4) The amount of ground motion on the geotechnical asset is vital. If the ground motion exceeds one-half the radar wavelength between each acquisition, the geotechnical asset will decorrelate and no information can be gained. There are three ways to avoid this problem: (1) acquire enough radar images for a temporally-dense stack, (2) use longer-wavelength radar data (e.g., ERS-1, ERS-2, ENVISAT, and RADARSAT-1 are all C-band satellites with $\lambda = 5.6$ cm, while ALOS PALSAR is an L-band satellite with $\lambda = 23.6$ cm), or (3) avoid trying to monitor geotechnical assets with high ground velocities with InSAR stacking techniques.

5.2 *LiDAR*

At the site-specific scale, detailed LiDAR surveys yield volumes of data. Repeated surveys from the same location, with established survey control, can be used to generate in-depth analysis to develop an understanding of specific geotechnical risks, such as slope stability. Geotechnical assets, such as bridges and retaining walls, are common assets monitored with LiDAR. Local-scale data are used to monitor, study, and mitigate changes observed in slopes, foundations, piers, and erosion from river scouring.

In Alaska and the Arctic, static terrestrial LiDAR are integral in understanding the effects of permafrost thaw associated with warming climates. Seasonal thaw ratchets soil downslope and causes foundations to shift. Ice lenses frozen for thousands of years are now melting creating sinkholes. And stabilizing geotechnical asset in this changing environment is critical to the operation and cost management of transportation assets, especially for pipelines, roads, bridges, and railroads. Another characteristic of close range laser scanning is the ability to fuse the LiDAR point cloud with colorized data from imagery collected at the same survey site, ideally from the same tripod used during the LiDAR scan. The fusion of the close-range digital imagery and LiDAR allows easier interpretation of the point cloud in order to understand complex geology of a road cut or bare slope (compare figures 13 and 14).

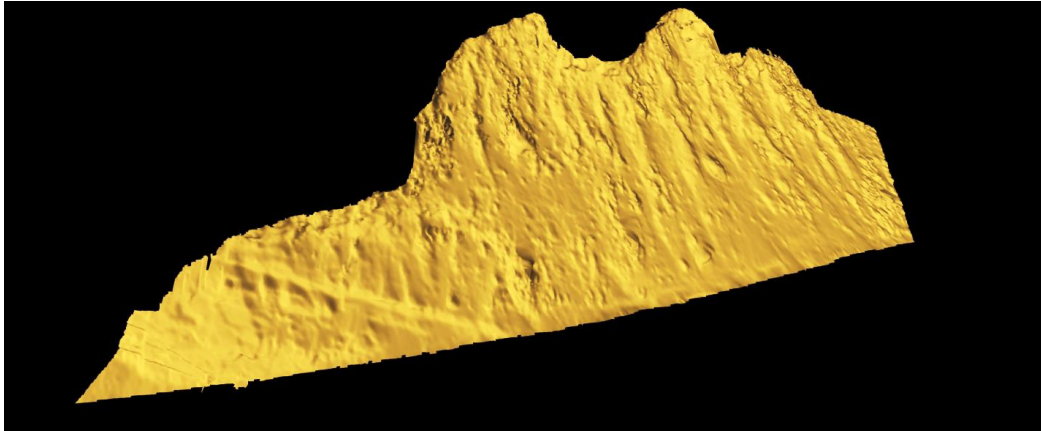


Figure 13. Example of a LiDAR surface mesh at the Glitter Gulch project site (from A Platform for Proactive, Risk-Based Slope Asset Management, Phase II, by Cunningham, Olsen and Wartman).

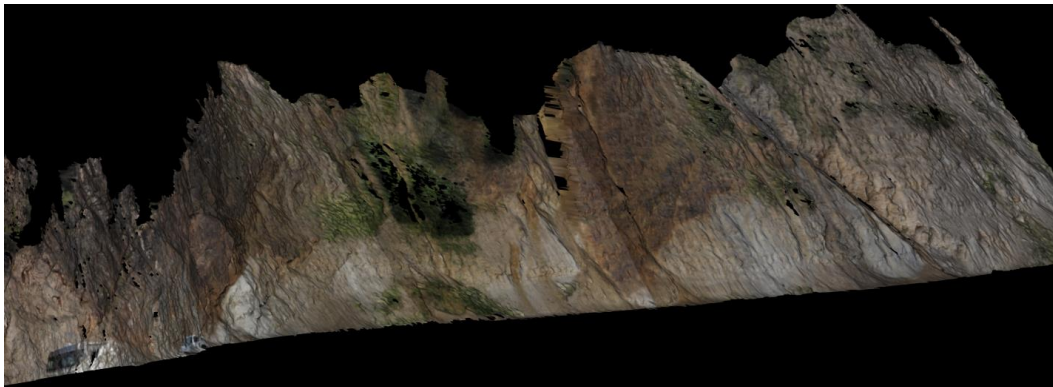


Figure 14. Example of the colorized LiDAR surface at the Glitter Gulch project site (from A Platform for Proactive, Risk-Based Slope Asset Management, Phase II, by Cunningham, Olsen and Wartman).

A limitation of local terrestrial LiDAR is it is presently limited to static terrestrial surveys, which means re-occupying known survey positions. However, some perspectives of a slope or feature may not be completely visible from the site specific view, creating data voids on some slopes. Another limitation is the density of the LiDAR positions decreases with distance from the LiDAR scanner, with densities as high as 10 postings per square centimeter close to the scanner and those densities quickly declining with distance and the incident angle of the laser scan (figure 15).

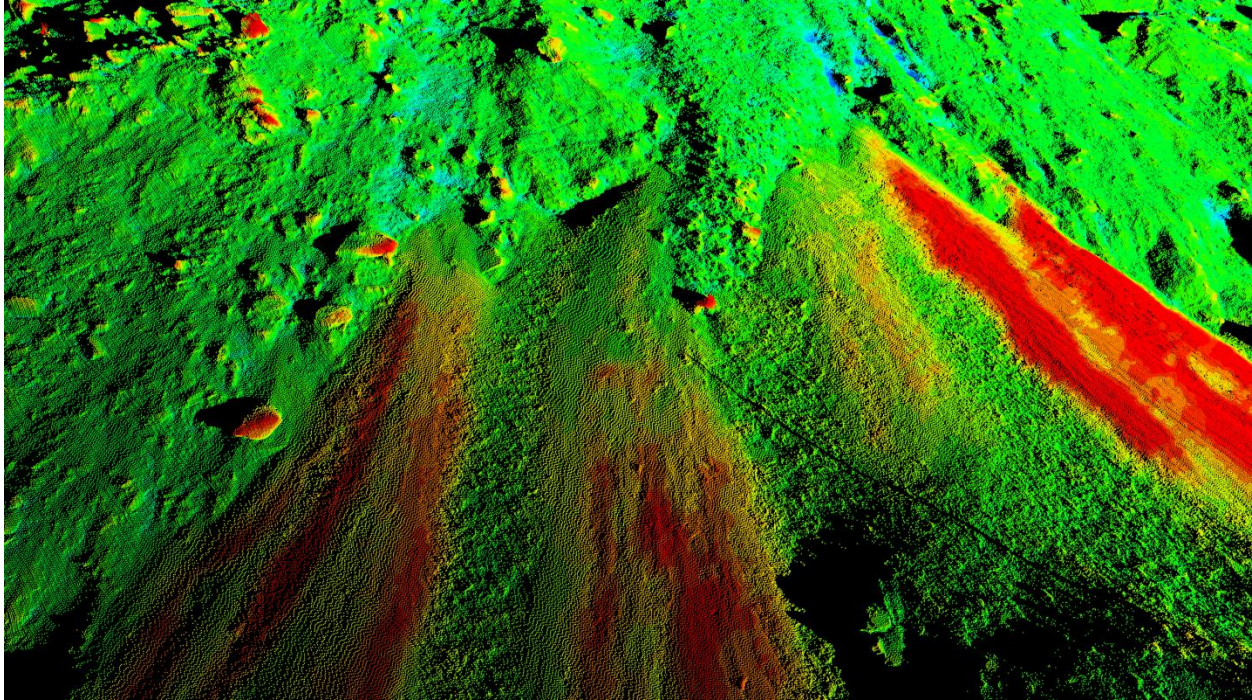


Figure 15. Change detection of two LiDAR data sets with erosion (<0.25m) in blue and accretion in red (>0.25m) (from A Platform for Proactive, Risk-Based Slope Asset Management, Phase II, by Cunningham, Olsen and Wartman).

5.3 Optical Photogrammetry

Local scale photogrammetry could utilize terrestrial and aerial platforms to collect imagery of assets. This could include the use of vehicles, UAVs, or even a hand held camera depending on the size of the area and accessibility. Using ground based (vehicle or terrestrial mounted) optical photogrammetry is less dependent upon weather conditions in comparison to UAV based remote sensing. Additionally, on a larger scale, the results obtained by optical remote sensing will have a higher resolution. However, the area being covered will be greatly reduced. Vehicle based optical sensing requires the use of road lanes, unobstructed by other drives and thus would need lane closures. On a local scale, remote sensing requirements for UAVs become less constraining due to the fact that flying at lower elevations reduces the impacts weather may have (but cannot be done during a precipitation event)

An example of a local application of the methods is given by Cerminaro (2014) in the context of retaining wall displacement monitoring. Periodic photo-surveys done over a one year period

were processed using photogrammetric methods (i. e. structure from motion algorithms), to produce displacement maps of retaining wall sections along the M-10 highway in Detroit, Michigan. Movements on the order of a few cm were recognizable in the data across some wall section joints (see figures 16, 17 and 18). The localized nature of the displacement suggests the failure of the retaining wall anchoring at specific locations, this information could guide the maintenance and repair work of specific sections along the retaining wall.

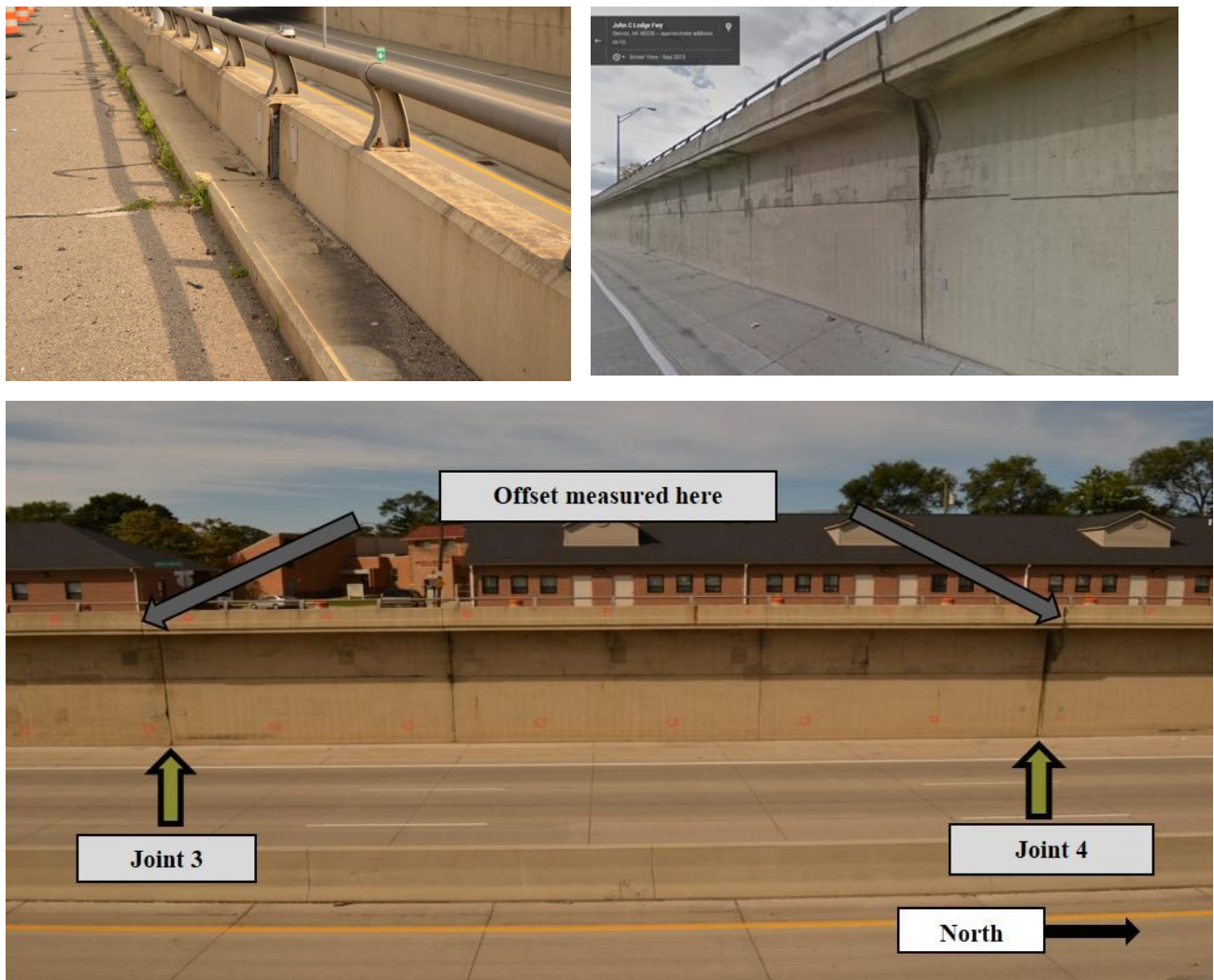


Figure 16. View of retaining wall joint along M-10 highway, suffering differential displacement, and which were surveyed using photogrammetric methods (adapted from Cerminaro, 2014). The upper left and right panels show the displacement at the joint on the back and front of the retaining wall sections, respectively. The lower panel shows the retaining wall sections and joints, as seen across the M-10 highway.

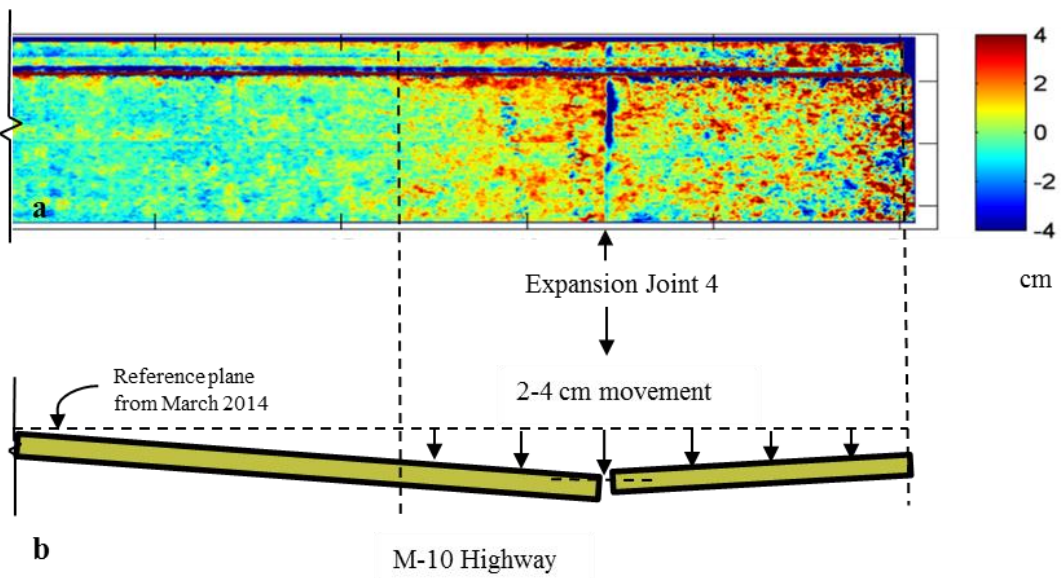


Figure 17. Retaining wall displacement on both sides of the joint, suggesting displacement of both sections of the retaining wall.

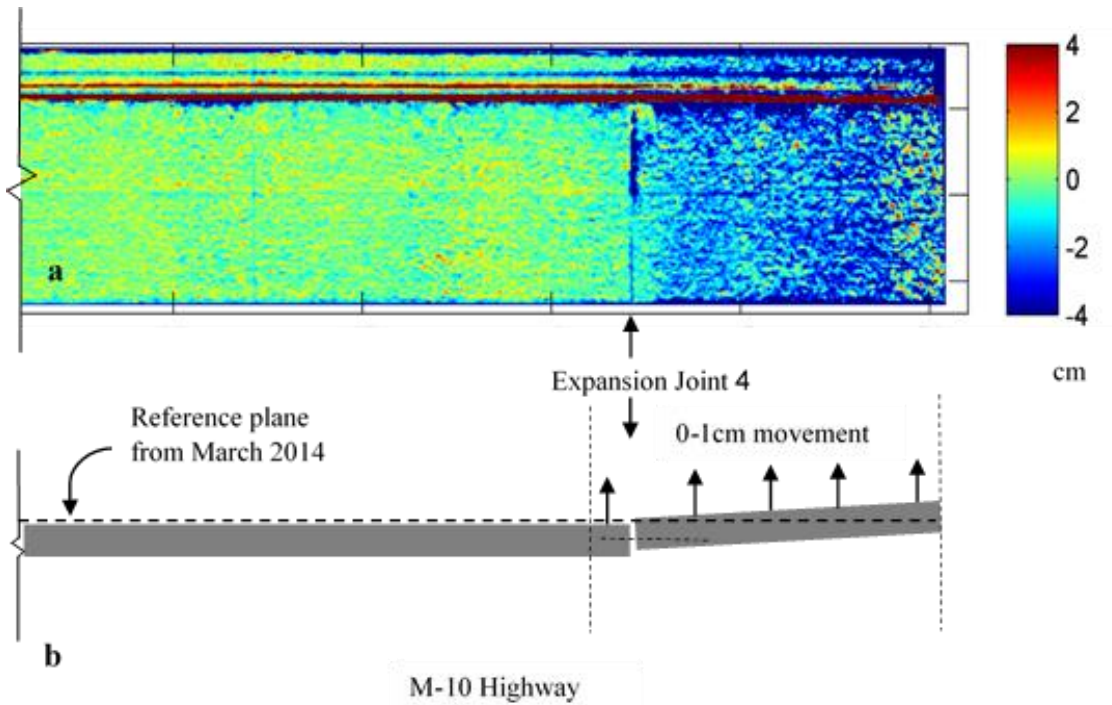


Figure 18. Retaining wall displacement on only one side of the expansion joint, suggests that only one of the retaining wall sections has failed, probably by rupture of a tension element behind the wall.

6. Remote sensing technologies rating

Following Ahlborn et al. (2010), we develop a relative rating of the different remote sensing methods discussed in previous sections. We limit our discussion to only the three main methods covered in those sections, focusing on their potential for detecting surface displacements over time, but we also consider other characteristics (see discussion below).

The rating is based on the perceived performance of the techniques, on a list of required or advantageous characteristics for the monitoring of geotechnical assets. A series of performance criteria are defined and a score for each criterion is chosen based on our evaluation of that method, following the discussion on the methods in the previous sections. Scores range from 1 (least adequate in meeting the criterion) to 3 (fully meets the criterion), and establish a relative ranking among remote sensing techniques, for each performance criterion.

Performance criteria were chosen after a review of the relevant literature, depending on the type of asset (e.g. Anderson et. Al., 2008; Vessely, 2013; Stanlye et. al., 2013), but focusing on the type of geotechnical information that is expected to be relevant for monitoring the assets, and the practical and material constraints for an agency in implementing such technologies. Criteria were ultimately condensed in only 7 indicators, for compactness and simplicity. To make criteria comparable, we normalized some of the extensive characteristics (e.g. costs) to what we estimate would be its value over a common area. Following is a description of the criteria and a general discussion on how they were applied to the specific remote sensing technology options.

Criterion A: Information content. The products from the different methods can all be used to estimate surface deformation over time. This measurement is highly relevant to the geotechnical monitoring of the asset, but other types of information, like panchromatic and multispectral electromagnetic intensity, do also contribute potentially useful information for characterizing other aspects of the asset, that may also be relevant for its geotechnical monitoring.

Both LiDAR and photogrammetric surveys of a slope can produce a point cloud with spatial information for each point (e. g. its x, y, and z spatial coordinates), but photogrammetry

additionally provides information of the target surface color (i.e. multispectral red-green-blue channels of the photographs), which can be used to assess other characteristics of the surface, like type of surface cover (e. g. vegetation, rock, etc.). LiDAR *per-se*, usually only returns a single band intensity per point, additional to the spatial information, and in that sense provides less information than photogrammetry does. However, current LiDAR instruments are commonly interfaced with high resolution photographic cameras, such that red-green-blue values from pictures taken during LiDAR scans can also be attached to each LiDAR point, providing a similar dataset to those produced by photogrammetry. InSAR on the other hand, does not provide such a multispectral information, although SAR provides polarimetric information, additionally to the intensity and phase information inherent in the radar dataset, that can be used independently of the ranging and interferometric information. By relating point information (e. g. for each pixel) in the SAR dataset, a map of spatial coherence can be obtained, which in itself also conveys information about the target surface (e. g. steady, non-changing like rock faces, vs unsteady and highly dynamic surfaces like vegetation).

Criterion B. Data spatial density and ground resolution.

The remote sensing techniques described in previous sections produce information that can be related to points in space, the density of those points in space (how close they are to each other) and the minimum values they can resolve of the characteristic that they are measuring (e. g. the minimum displacement that they can measure), are very important in assessing the value of the technology for geotechnical asset monitoring. Such data density and resolution may vary depending on the application platform for a given technology, e.g. aerial LiDAR will have a lower point density than terrestrial, static LiDAR, and a similar consideration applies to photogrammetry. For LiDAR and photogrammetry the point densities on the target surface are usually on the order of thousands to at least one point per m². Satellite based InSAR as discussed in this report, will in general have a much lower data density (up to a few points per m², for the most recent sensor), and its point resolution for detecting ground displacement can be similar or even better (< 5 mm) than LiDAR and photogrammetry (> 1 cm). InSAR from other platforms can have much higher spatial point density, depending on the distance to the target. Static terrestrial LiDAR and photogrammetry, and UAV based photogrammetry are considered for the purpose of this evaluation.

Criterion C. Data availability and time interval recurrence.

Data availability is linked with the capacity of the user to collect and generate its own dataset, or its dependence on other sources to collect and generate the data. LiDAR and photogrammetry datasets are considered to be available to within operational limitations of the user, or the provider of the service that the user contracts for that purpose, and so they can be collected over the areas of interest, as often as the service provider and the budget allows. For a user with the capacity to collect and generate its own data, this can be as frequent as daily, for monitoring rapidly changing phenomena (e. g. active landslides), and over relatively extensive areas (especially in the case of sensors based on aerial or UAV platforms). This allows for a greater flexibility of data collection for specific areas, during specific times. Environmental and physical limitations, include good weather conditions (especially for aerial and UAV platforms), and good visibility (and lighting) conditions, especially for photogrammetry.

Satellite based InSAR on the other hand is dependent on the satellite's acquisition schedule, which is usually outside the reach of the user. Data availability for some areas can be expected to be on the order of tens of scenes per year, while for other areas there may not be any scenes at all. Historic satellites (ESR-1/-2, ENVISAT) were on a 35-day revisit schedule, but once the Sentinel constellation of satellites is launched, they expect a revisit period of 3 days.

Criterion D. Accuracy

Closely linked to the data density and resolution, the concept of accuracy describes how close the measurements are to the real value of the characteristics of the object being measured. Additionally to errors introduced in the measuring process, the need for reference frames, like the choice of a reference point in the InSAR displacement analysis, or the choice of ground control points for photogrammetry, introduces additional uncertainty and errors in the measured quantities.

These affects are minimal on single terrestrial LiDAR scans, for a correctly calibrated and functioning instrument. But the overall accuracy of multiple LiDAR scans that need to be tied through control points and targets, or the position of LiDAR points acquired from moving

platforms (e. g. mobile terrestrial, aerial and UAV), is highly dependent on the GPS and inertial location systems used to georeference the datasets. Photogrammetry invariably relies on good control points, and the impact of the number, distribution and accuracy of those points has a large impact on the accuracy of the photogrammetric output. Depending on terrain accessibility, locating and surveying enough control points can quickly increase the cost of data collection. Satellite based InSAR is also subject to several sources of error (atmospheric effects, orbital uncertainty, etc.), that are usually modeled and accounted for during data processing and analysis. The choice of the relative reference for comparing InSAR displacement data over time is particularly critical, as this can influence the whole time series making the entire dataset highly sensitive to this choice.

Criterion E. Direct cost for data collection and analysis

The direct costs involved in data collection and analysis can vary depending on whether the user develops its own capabilities to do so (increasing indirect costs and requiring a longer term investment) or outsources the service to a contractor. LiDAR and photogrammetry costs are mainly related to fieldwork data collection, and analysis time (analyst, software license, etc.) for data processing. Fieldwork in both cases is comparable, and a large portion of it consist in deploying and surveying the control points that will be used in tying and georeferencing the different LiDAR scans or photograph blocks. Aerial data collection is more expensive but covers much more ground for a given amount of time, offsetting the cost per area of surveyed terrain. Data processing and analysis in both cases is also comparable. Satellite based InSAR data have to be purchased at a relatively high global costs (per image), but they also cover a very large area, resulting in a relatively low cost per km², this implies that InSAR data become more cost effective as the area of interest becomes larger. The cost of InSAR data processing and analysis is also comparable to that of LiDAR and photogrammetry.

Criterion F. Indirect cost for data collection and analysis

Indirect costs for the different remote sensing technologies are related to the investment in instrumentation and training on the data analysis and interpretation. LiDAR instruments, range in price from a few tens of thousands of dollars, to more than 100,000. Photogrammetry on the other hand, relies on relatively inexpensive (< 5,000 dollars) digital single-lens-reflex digital

cameras. The platform for the sensor can add to the cost, from non-additional cost for terrestrial LiDAR or photogrammetry, to the cost of contracting (or even buying) and aircraft for aerial surveys. Photogrammetry offers the possibility to use inexpensive (< 10,000 dollars) UAV, which offer an option in between terrestrial and fully aerial surveys. Instrument and platform considerations don't apply to the satellite based InSAR case. Software for data analysis are within a similar price range for LiDAR, photogrammetry and InSAR analysis (< 10,000 dollars).

Criterion G. Availability of historical data.

Although data collection for the different methods in many cases could be done by the user (e. g. through LiDAR or photogrammetry collection campaigns), in some cases the existence of prior data is also very informative and useful. For long-term monitoring of geotechnical assets it is important to establish long-term baselines of the behavior and performance of the asset, and unless this had been done by the user over an extended period of time, other sources of information will be necessary to try to establish such long-term behavior. In the case of LiDAR, give its relatively young age as a surveying technology and the rather focused nature of its data collection, e. g. most commonly done only in areas where a specific target is defined (e. g. a specific asset or structure) and driven a particular goal (surveying for earth movement, constructions, etc.), it is hard to find datasets taken by other agencies or companies by chance, and that would be available to the public. In some cases, government, have collected such data, usually from aerial platforms and have made them available to the public. The number of datasets available per site usually is restricted to only one or two.

Aerial photography and actual stereophotogrammetric pairs are more commonly available, as this technology has existed and has been employed since the 1940's. Electronic image archives maintained by the USGS and similar government agencies provide moderate resolution imagery (e. g. 0.5 – 2 m pixel resolution) for large areas of the US, including datasets from several times over the last few decades (although data tend to be more frequent in more recent times). Some of the datasets directly available to the public through download links on the agencies websites have been orthorectified, rendering them useless for photogrammetric purposes, however the original datasets are almost always available upon request from the hosting agencies (usually at some additional cost for the user). The option to request the original photography data from the

agencies also allows in some cases to request higher scanning resolutions (< 0.5 m pixel size), allowing for better surface models to be created from these images.

InSAR data have been acquired from satellite platforms since the 1990's, providing a long running archive of radar images for some sites. Despite some data-gaps in recent years, the satellite based InSAR archive can be used to assess the long-term stability of geotechnical assets through the monitoring of the asset surface displacement, on the order of a few mm, over more than two decades. Based on the criteria discussed in the previous paragraphs, we assign the scores shown in table 2.

Table 2. Performance rating for the 3 remote sensing technologies

Criterion	LiDAR	Photogrammetry	InSAR
A. Information content	3	3	3
B. Data spatial density and ground resolution	3	3	2
C. Data availability and time interval recurrence	3	3	2
D. Accuracy	3	3	3
E. Direct cost for data collection and analysis	2	2	3
F. Indirect cost for data collection and analysis	1	3	3
G. Availability of historical data	1	2	3

7. Conclusion

Geotechnical assets, such as retaining walls, embankments, cut slopes, and rock slopes are indispensable components for healthy transportation infrastructure. According to the American Association of State Highway and Transportation Officials' (AASHTO) Transportation Asset Management Guide, over the past decade there has been a growing awareness that the current methods of transportation infrastructure management are not adequate to meet the demands of the public and therefore, need improvement (AASHTO 2013).

Current practices for managing geotechnical assets along transportation corridors are mostly focused on restoring the asset after failure, as opposed to identifying and remediating hazardous conditions before their occurrence. One of the reasons for lacking a proactive system is, geotechnical assets are extensive and assessing their condition using traditional site inspection is mostly qualitative and laborious.

In this report, we rated the applicability of three remote sensing techniques (InSAR, LiDAR, and Photogrammetry) for geotechnical asset management based on different criteria, such as:

- Information content
- Data spatial density and ground resolution
- Data availability and time interval recurrence
- Accuracy
- Direct cost for data collection and analysis
- Indirect cost for data collection and analysis
- Availability of historic data

Results indicate that there is no technique that has high rating for all criteria. In general, the photogrammetry method is the most cost effective and easy to process, whereas, the InSAR method has the relatively low cost per km² and can provide mm scale accuracy. The LiDAR and photogrammetry are comparable except that the initial cost for LiDAR instrumentation can be significantly higher. The detailed rating results presented in Table 2 highlight the criteria of the remote sensing techniques that have potential to impact the current practices for geotechnical asset management, and also the ones that need additional sensor development and commercialization. Ongoing and future activities of this study will investigate the field performance of these remote sensing techniques for geotechnical asset management.

8. References

- AASHTO (2011). Transportation Asset Management Guide, Volume 2: A Focus on Implementation." American Association of State Highway and Transportation Officials. Prepared under NCHRP Project. 69 pp.
- Ahlborn, T. M., R. Shuchman, L. L. Sutter, C. N. Brooks, D. K. Harris, J. W. Burns, K. A. Endsley, D. C. Evans, K. Vaghefi, and R. C. Oats. (2010) "An Evaluation of Commercially Available Remote Sensors for Assessing Highway Bridge Condition." Report to the US Department of Transportation. 73 pp.
- Ahmed, R.; Siqueira, P.; Henlsey, S.; Chapman, B.; Bergen, K. (2011) A survey of temporal decorrelation from spaceborne L-Band repeat-pass InSAR. *Remote Sensing of Environment*. 115(11), 2887-2896.
- Anderson, Scott A., Daniel Alzamora, and Matthew J. DeMarco. (2008) "Asset Management Systems for Retaining Walls." *GEO-Development. The Role of Geological and Geotechnical Engineering in New and Redevelopment Projects*. ASCE. 162-177.
- Anderson, Scott A., and Benjamin S. Rivers. (2013) "Capturing The Impacts of Geotechnical Features on Transportation System Performance." *Geo-Congress Stability and Performance of Slopes and Embankments III*. ASCE. 1633-1642.
- Askne, J.I.H.; Dammert, P.B.G.; Ulander, L.M.H.; Smith, G. (1997) C-Band Repeat-Pass Interferometric SAR Observations of the Forest. *IEEE Transactions on Geoscience and Remote Sensing*. 35(1), 25-35.
- Bamler, R. & Hartl, P. (1998) Synthetic aperture radar interferometry. *Inverse Problems*. 14, R1-R54.
- Bayer, T.; Winter, R.; Schreier, G. (1991) Terrain Influences in SAR Backscatter and Attempts to their Correction. *IEEE Transactions on Geosciences and Remote Sensing*. 29(3), 451-462.
- Bürgmann, R.; Hilley, G.; Ferretti, A.; Novali, F. (2006) Resolving vertical tectonics in the San Francisco Bay Area from permanent scatterer InSAR and GPS analysis. *Geology*. 34(3), 221-224. doi: 10.1130/G22064.1.
- Cambridge Systematics. (2002) "Transportation Asset Management Guide, Task I—Synthesis of Asset Management Practice."
- Cerminaro, (2014). Implementation of photogrammetry to improve proactive assessment of retaining walls along transportation corridors. Master's Thesis. Michigan Technological University. 68 pp.
- Crosetto, M., Monserrat, O.; Iglesias, R.; Crippa, B. (2010) Persistent scatterer interferometry: Potential, limits and initial C- and X-band comparison. *Photogrammetric Engineering and Remote Sensing*. 76(9), 1061-1069.
- Cunningham, K., Olsen, M., Wartman, J., Dunham, L., Stuedlein, A. (2014) A Platform for Proactive Risk-Based Slope Asset Management: Phase II. *Pacific Northwest Transportation Consortium*. Draft report.
- Desnos, Y.-L.; Buck, C., Guijarro, J.; Suchail, J.-L.; Torres, R.; Attema, E. (2010) ASAR – Envisat's Advanced Synthetic Aperture Radar: Building on ERS Achievements towards Future Earth Watch Missions. *ESA Bulletin 102 – May 2010*. 91-100.
- Dubois, P.C.; van Zyl, J.; Engman, T. (1995) Measuring Soil Moisture with Imaging Radars. *IEEE Transactions on Geoscience and Remote Sensing*. 33(4), 915-926.

- Duffell, C. G., and D. M. Rudrum. (2005) "Remote sensing techniques for highway earthworks assessment." *Proceedings of GeoFrontiers*. 1-13.
- Dzurisin, D. & Lu, Z. (2007) Interferometric Synthetic Aperture Radar (InSAR) (Chapter 5), in *Volcanic Deformation: Geodetic Monitoring Techniques*, by D. Dzurisin, Springer-Praxis Publishing Ltd., UK, 42 pages.
- European Space Agency (ESA) (2002a) Envisat Instruments. <https://earth.esa.int/instruments/>.
- European Space Agency (ESA) (2002b) RADARSAT-1. <https://directory.eoportal.org/web/eoportal/satellite-missions/r/radarsat-1>
- European Space Agency (ESA) (2008) ERS-2 InSAR Restored to Life: Zero-Gyro Mode and Tandem Operation with ENVISAT. *The Living Planet* [Brochure], 1-15.
- European Space Agency (ESA) (2012) ENVISAT. http://www.esa.int/Our_Activities/Operations/Envisat.
- European Space Agency (ESA) (2013) MERIS Products. <http://earth.esa.int/instruments/meris/data-app/dataprod.html>.
- Ferretti, A.; Prati, C.; Rocca, F. (2000) Nonlinear subsidence rate estimation using permanent scatterers in differential SAR interferometry. *IEEE Transactions on Geoscience and Remote Sensing*. 38(5), 2202-2212.
- Ferretti, A.; Prati, C.; Rocca F. (2001) Permanent Scatterers in SAR Interferometry. *IEEE Transactions on Geoscience and Remote Sensing*. 39(1), 8-20.
- Ferretti, A.; Fumagalli, A.; Novali, F.; Prati, C.; Rocca, F.; Rucci, A. (2011) A New Algorithm for Processing Interferometric Data-Stacks: SqueeSAR. *IEEE Transactions on Geoscience and Remote Sensing*. 49(9), 3460-3470.
- Freeman, T. & Wong, A. (1996) What is Imaging Radar? <http://southport.jpl.nasa.gov/GRFM/cdrom/2b/DOCS/HTML/IMGV3.HTM>.
- Hooper, A.; Zebkar, H.; Segall, P.; Kampes, B. (2004) A new method for measuring deformation on volcanoes and other non-urban areas using InSAR persistent scatterers. *Geophysics Research Letters*. 31(23), 1-5.
- Kampes, B.M.; Hanssen, R.F.; Perski, Z. (2003) Radar interferometry with public domain tools. *Proceedings from FRINGE*. <http://doris.tudelft.nl/Literature/kampes03b.pdf>.
- Kohlhase, A.O.; Feigl, K.L.; Massonnet, D. (2003) Applying differential InSAR to orbital dynamics: a new approach for estimating ERS trajectories. *Journal of Geodesy*. 77, 493-502. doi: 10.1007/s00190-003-0336-3.
- Lin, Q.; Vesecky, J.F.; Zebker, H.A. (1994) Phase unwrapping through fringe-line detection in synthetic aperture radar interferometry. *Applied Optics*. 33, 201-208.
- Lopes, A.; Nezry, E.; Touzi, R., Laur, H. (1993) Structure detection and statistical adaptive speckle filtering in SAR images. *International Journal of Remote Sensing*. 14(9), 1735-1758.
- Massonnet, D.; Rossi, M.; Carmona, C.; Adragna, F.; Peltzer, G.; Fiegl, K.; Rabaute, T. (1993) The displacement field of the Landers earthquake mapped by radar interferometry. *Nature*. 364, 138-142. doi: 10.1038/364138a0.
- Massonnet, D.; Briole, P.; Arnaud, A. (1995) Deflation of Mount Etna monitored by spaceborne radar interferometry. *Nature*. 375, 567-570. doi: 10.1038/375567a0.
- Stanley, David A., and Lawrence A. Pierson. "Geotechnical Asset Management of Slopes: Condition Indices and Performance Measures." *Geo-Congress 2013 Stability and Performance of Slopes and Embankments III*. ASCE. 1651-1660.
- Wolff, C. (1998) Synthetic Aperture Radar. <http://www.radartutorial.eu/20/airborne/ab07.en.html>.